Identification and transcriptomic profiling of salinity stress response genes in colored wheat mutant

Min Jeong Hong [1], **Chan Seop Ko** [1], **Jin-Baek Kim** [1], **Dae Yeon Kim** Corresp. [2]

[1] Advanced Radiation Technology Institute, Korea Atomic Energy Research institute, Jeongeup, Jeollabuk-do, Korea

[2] Plant Resources, Kongju National University, Yesan-eup, Chungnam, South Korea

Corresponding Author: Dae Yeon Kim
Email address: dykim@kongju.ac.kr

Background. Salinity is a major abiotic stress that prevents normal plant growth and development, ultimately reducing crop productivity. This study investigated the effects of salinity stress on two wheat lines: PL1 (wild type) and PL6 (mutant line generated through gamma irradiation of PL1). **Results.** The salinity treatment was carried out with a solution consisting of a total volume of 200 mL containing 150 mM NaCl. Salinity stress negatively impacted germination and plant growth in both lines, but PL6 exhibited higher tolerance.

PL6 showed lower Na^+ accumulation and higher K^+ levels, indicating better ion homeostasis. Genome-wide transcriptomic analysis revealed distinct gene expression patterns between PL1 and PL6 under salt stress, resulting in notable phenotypic differences. Gene ontology analysis revealed positive correlations between salt stress and defense response, glutathione metabolism, peroxidase activity, and reactive oxygen species metabolic processes, highlighting the importance of antioxidant activities in salt tolerance. Additionally, hormone-related genes, transcription factors, and protein kinases showed differential expression, suggesting their roles in the differential salt stress response. Enrichment of pathways related to flavonoid biosynthesis and secondary metabolite biosynthesis in PL6 may contribute to its enhanced antioxidant activities. Furthermore, differentially expressed genes associated with the circadian clock system, cytoskeleton organization, and cell wall organization shed light on the plant's response to salt stress. **Conclusions.** Understanding these mechanisms is crucial for developing stress-tolerant crop varieties, improving agricultural practices, and breeding salt-resistant crops to enhance global food production and address food security challenges.

Identification and Transcriptomic Profiling of Salinity Stress Response Genes in Colored Wheat Mutant

Min Jeong Hong[1], Chan Seop Ko[1], Jin-Baek Kim[1]
[1] Advanced Radiation Technology Institute, Korea Atomic Energy Research Institute, 29 Geumgu, Jeongeup 56212, Korea

Corresponding Author:
Dae Yeon Kim[2]
[2] Department of Plant Resources, Kongju National University, 54 Daehak-ro Yesan-eup Chungnam 322439, Korea
Email Address dykim@kongju.ac.kr

Abstract

Background. Salinity is a major abiotic stress that prevents normal plant growth and development, ultimately reducing crop productivity. This study investigated the effects of salinity stress on two wheat lines: PL1 (wild type) and PL6 (mutant line generated through gamma irradiation of PL1).

Results. The salinity treatment was carried out with a solution consisting of a total volume of 200 mL containing 150 mM NaCl. Salinity stress negatively impacted germination and plant growth in both lines, but PL6 exhibited higher tolerance. PL6 showed lower Na^+ accumulation and higher K^+ levels, indicating better ion homeostasis. Genome-wide transcriptomic analysis revealed distinct gene expression patterns between PL1 and PL6 under salt stress, resulting in notable phenotypic differences. Gene ontology analysis revealed positive correlations between salt stress and defense response, glutathione metabolism, peroxidase activity, and reactive oxygen species metabolic processes, highlighting the importance of antioxidant activities in salt tolerance. Additionally, hormone-related genes, transcription factors, and protein kinases showed differential expression, suggesting their roles in the differential salt stress response. Enrichment of pathways related to flavonoid biosynthesis and secondary metabolite biosynthesis in PL6 may contribute to its enhanced antioxidant activities. Furthermore, differentially expressed genes associated with the circadian clock system, cytoskeleton organization, and cell wall organization shed light on the plant's response to salt stress.

Conclusions. Understanding these mechanisms is crucial for developing stress-tolerant crop varieties, improving agricultural practices, and breeding salt-resistant crops to enhance global food production and address food security challenges.

Introduction

Wheat is a crucial crop cultivated globally, contributing to 30% of global grain production and providing approximately 20% of the calories consumed by humans (*Shiferaw et al*., *2013*; *Seleiman et al*., *2022*). Soil salinity poses a critical issue, resulting in yield losses of up to 60% in wheat production (*El-Hendawy et al*., *2017*). Salinity stress disrupts plant growth by increasing Na^+ ion assimilation and reducing the Na^+/K^+ ratio, leading to osmotic stress and ion toxicity, consequently affecting normal plant development (*EL Sabagh et al*., *2021*). Additionally, under salinity stress, oxidative stress can impair plant growth through reduced photosynthetic capacity, oxidative damage caused by an imbalance in reactive oxygen species (ROS) production, and decreased antioxidant activity, ultimately leading to reduced crop yield (*Hasanuzzaman et al*., *2014*; *Sadak*, *2019*; *Omrani et al*., *2022*).

Climate change and global warming cause various environmental stresses, such as temperature fluctuations, droughts, floods, and increased salinity, which have detrimental effects on crop productivity (*Kissoudis et al*., *2014*). Among these stresses, salinity stress is a significant abiotic factor that hampers plant growth and development, leading to decreased agricultural productivity (*Amirbakhtiar et al*., *2019*; *Al-Ashkar et al*., *2019*). The impact of salinity is extensive, with >20% of irrigated land worldwide being affected (*EL Sabagh et al*., *2021*). Furthermore, it is projected that up to 50% of arable land will be lost by 2050 owing to salinization caused by both human

activities and ongoing climate change (*Asif et al*., *2018*; *Kumar & Sharma*, *2020*; *Chele et al*., *2021*).

Numerous studies have focused on breeding new salt-tolerant crop varieties using molecular and biology-based technologies (*Huang et al*., *2008*; *Ismail & Horie*, *2017*; *Saade et al*., *2020*; *Hussain et al*., *2021*) and on selecting salt-tolerant crops. These selection criteria encompass germination rate (*El-Hendawy et al*., *2019*; *Choudhary et al*., *2021*), plant growth (*Sayed*, *1985*), chlorophyll content (*Tsai et al*., *2019*), and K^+/Na^+ ratio (*Assaha et al*., *2017*; *Singh & Sarkar*, *2014*). Particularly, the germination and growth rates during the early stages of plant development have proven useful for screening salt-tolerant crops (*Choudhary et al*., *2021*). In *Brassica napus*, root and shoot lengths act as early indicators for evaluating salt tolerance (*Long et al*., *2015*). In rice, salt-tolerant cultivars have higher chlorophyll content and Na^+/K^+ ratios under salt stress conditions than salt-susceptible cultivars (*Singh & Sarkar*, *2014*). Regulating excessive Na^+ accumulation in plants is a vital strategy for enhancing salt resistance (*Tester & Davenport*, *2003*; *Møller & Tester*, *2007*; *Møller et al*., *2009*). The high-affinity K^+ transporter (HKT) gene family plays a crucial role in maintaining Na^+ and K^+ balance in plant growth, development, abiotic stress responses, and salt tolerance (*Horie et al*., *2009*; *Li et al*., *2019*; *Riedelsberger et al*., *2021*). Initially identified in wheat (*Schachtman & Schroeder*, *1994*), HKT genes have been found to reduce Na^+ accumulation in higher plants, such as *Arabidopsis*, rice, and wheat (*Riedelsberger et al*., *2021*). Additionally, the salt overly sensitive (SOS) gene family is involved in regulating ion homeostasis and Na^+ exclusion at the cellular level, affecting plant salinity tolerance (*Yang et al*., *2009*).

Despite ongoing research on gene regulation under salt stress, limited progress has been made in establishing appropriate screening methods using genetic resources, understanding mechanisms underlying osmotic stress/tissue resistance, and identifying salt-tolerant crops (*Genc et al*., *2019*). Furthermore, as elite germplasm may lack genes that confer salt resistance, genetic engineering involving the artificial insertion of specific genes may be required to develop new crop varieties (*Colmer et al*., *2006*; *Shavrukov et al*., *2009*; *Munns et al*., *2012*; *Deinlein et al*., *2014*).

Genetic diversity is crucial for developing new and improved crop varieties with desirable traits. However, breeders often focus on improving traits by selecting offspring with the best attributes, leading to a decrease in genetic diversity when some plants become vulnerable to environmental stresses. Mutation breeding is a widely used method for enhancing genetic diversity and improving crop traits. Gamma rays, being physical mutagens, are commonly used for plant mutation breeding and have been instrumental in developing >50% of the 3,401 new varieties included in the FAO/IAEA Mutant Variety Database (https://nucleus.iaea.org/sites/mvd/SitePages/Home.aspx). In light of these findings, the construction of a mutant pool using gamma rays offers an opportunity to develop salt-resistant wheat by securing genetic diversity. Therefore, this study selected the salt-resistant colored wheat mutant PL6 (developed via gamma ray mutagenesis) and investigated its salt resistance mechanism induced by gamma ray mutation through transcriptome analysis of PL6 and wild-type (PL1) wheat. Breeding salt-tolerant crops is challenging owing to the complexity of

polygenic traits resulting from genetic and physiological diversity (*Genc et al*., *2019*; *Hanin et al*., *2016*). The findings of this study provide valuable insights for breeding salt-tolerant wheat and offer various interpretations of salt tolerance.

Materials & methods

Plant materials

In this study, we incorporated the common wheat (*Triticum aestivum* L., 2n= 6x= 42, AABBDD) inbred line K4191, which possesses deep purple grain color. K4191 (hereafter termed PL1) was derived from the $F_{4:8}$ generation resulting from the cross between 'Woori-mil' (obtained from the National Agrobiodiversity Center, RDA, Korea; accession no. IT172221) and 'D-7' (an inbred line developed by Korea University; Fleming4/3/PIO2580//T831032/Hamlet) (*Hong et al*., *2019*). To induce genetic variation and diversify the population of colored wheat, colored wheat seeds (PL1) were irradiated with 200 Gy gamma rays at a dose rate of 25 Gy/h using a ^{60}Co gamma irradiator (150 TBq of capacity; Noridon, Ottawa, ON, Canada) at the Korea Atomic Energy Research Institute. Subsequently, the irradiated seeds were planted at the radiation breeding research farm. Briefly, 1500 M_0 seeds were exposed to irradiation, and the resulting seeds were sown to generate the M_1 generation. Among these seeds, 287 phenotypically distinctive lines were carefully selected with one spike per plant, and mutation breeding spanning from M_0 to M_4 was performed as thoroughly described in a previous study (*Hong et al*., *2019*). The resulting mutants were continuously cultivated up to the M_6 generation and carefully selected based on excellent agricultural traits, including flowering time, plant height, yield, and grain color. In total, 50 mutant lines displaying stable phenotypes for at least two generations were chosen for further salt-tolerance screening.

Salt stress treatment

The PL1 (control line, K4191) and PL6 (mutant line) seeds were surface-sterilized with 70% ethanol for 1 min and then washed with sterile distilled water. Subsequently, the seeds were placed on moist filter papers in a Petri dish (SPL Life Sciences) until the first leaf of the seedlings appeared. Next, the uniformly germinated seeds were transferred to Incu Tissue culture vessels (SPL Life Sciences) filled with half-strength Hoagland's culture solution (Sigma-Aldrich, St. Louis, MO, USA). The solutions were replaced daily. The seedlings were grown for 7 days in a well-controlled chamber at 22°C and 60% humidity, with a photoperiod regime of 16/8 h day/night at 200–300 μmol $m^{-2}s^{-1}$ light. After 7 days of transplanting, the seedlings were subjected to a salt stress treatment of a total volume of 200 mL of the solution containing 150 mM NaCl. Following treatment with 150 mM NaCl, the wheat leaves were collected at 0, 3, 24, and 48 h. Both control and salt-stressed seedlings were collected individually. The samples were immediately frozen in liquid nitrogen and stored at −80°C until use in further experiments.

Measurement of leaf Na^+ and K^+ contents

The wheat leaves were collected separately and immediately frozen in liquid nitrogen. Subsequently, the samples were freeze-dried for 3 days in a Freeze Dry System (IlshinBioBase, Dongducheonsi, Gyeongi, Korea). The freeze-dried samples were then finely ground into a powder using a mortar and pestle. For further analysis, 50 mg of the freeze-dried samples was weighed

using an analytical balance and boiled for 2 h at 200°C in 3 mL of HNO_3 (70%, v/v) for digestion. After digestion, the extracted samples were diluted with 5% HNO_3 and filtered through a hydrophilic polytetrafluoroethylene syringe filter (0.45-μM pore size, 25-mm diameter). The shoot Na^+ and K^+ contents were measured using inductively coupled plasma atomic emission spectroscopy (ICP-AES, 720 series; Agilent, Santa Clara, CA, USA) and quantitatively analyzed using a VistaChip Ⅱ CCD detector (Agilent).

Measurement of chlorophyll content

To determine the chlorophyll content, wheat seedling samples were extracted with 100% methanol at 4°C. The sample extracts were then subjected to centrifugation at 12,000 ×*g* for 10 min, and the supernatant was used for chlorophyll content analysis. The total chlorophyll, chlorophyll a, and chlorophyll b concentrations were determined by measuring the absorbance at 644.8 and 661.6 nm using a UV-VIS spectrophotometer (*Lichtenthaler*, *1987*). The chlorophyll concentration was calculated using the following equations:

$$C_a = 11.24 \times A_{661.6} - 2.04 \times A_{644.8}$$

$$C_b = 20.13 \times A_{644.8} - 4.19 \times A_{661.6}$$

$$C_{total} = 7.05 \times A_{661.6} + 18.09 \times A_{644.8}$$

where C_a, C_b, and C_{total} denote the concentrations of chlorophyll a, chlorophyll b, and total chlorophyll, respectively.

RNA sequencing and gene expression analyses

Total RNA was extracted from the wheat leaves of both PL1 and PL6 at each timepoint (0, 3, 24, and 48 h) using TRIzol (Invitrogen, Carlsbad, CA, USA) following the manufacturer's instructions. Two independent biological replicates were performed for each timepoint and line to ensure the reliability and reproducibility of the RNA-seq data. Additionally, the extracted RNA samples were treated with DNase I to remove any potential genomic DNA contamination. The RNA quality was assessed using an Agilent 2100 bioanalyzer (Agilent Technologies, Amstelveen, The Netherlands), and RNA quantification was performed using an ND-2000 Spectrophotometer (Thermo Inc.; Wilmington, DE, USA). For constructing the RNA-seq paired-end libraries, 10 μg of total RNA extracted from the samples was used with the TruSeq RNA Sample Preparation Kit (Catalog #RS-122-2001; Illumina, San Diego, CA, USA). The mRNA was isolated using a Poly(A) RNA Selection Kit (LEXOGEN, Inc.; Vienna, Austria) and reverse-transcribed into cDNA following the manufacturer's instructions. The libraries were assessed using the Agilent 2100 bioanalyzer, and the mean fragment size was evaluated using a DNA High Sensitivity Kit (Agilent, Santa Clara, CA, USA). High-throughput sequencing was conducted using the HiSeq 2000 platform (Illumina). Before alignment, adaptor sequences were removed, and sequence quality was evaluated using the Bbduk tool (minimum length > 20 and Q > 20; https://jgi.doe.gov/data-and-tools/software-tools/bbtools/bb-tools-user-guide/bbduk-guide/). The reads were aligned to the wheat genome sequence provided by the International Wheat Genome Sequencing Consortium (IWGSC) wheat reference sequence (IWGSC Reference Sequence v1.0; https://urgi.versailles.inra.fr/download/iwgsc/IWGSC_RefSeq_Annotations/v1.0/) using the HISAT2 alignment program with default parameters (*Kim et al*., *2015*). Reads mapped to the exons

of each gene were enumerated using the HTSeq v0.6.1 high-throughput sequencing framework (*Anders et al*., *2015*). Subsequently, the differentially expressed genes (DEGs) under salt stress and control conditions were identified using the EdgeR package (*Robinson et al*., *2010*). Upregulated and downregulated genes with a p-value of <0.05, false discovery rate (FDR) of <0.05, and an absolute fold change value of >2 were used for downstream functional analysis. The log2-transformed transcript per million values were calculated using TPMCalculator (*Vera Alvarez et al*., *2019*), and heatmaps of DEGs under control and stress conditions were generated. Local BlastX was used with peptide sequences of the Poaceae family retrieved from the National Center for Biotechnology Information (NCBI) database using an e-value threshold of 1×10^{-5} to annotate the DEGs. For gene expression analysis, total RNA was used to synthesize first-strand cDNA using the Power cDNA Synthesis Kit (iNtRON Biotechnology, Gyeonggi-do, Korea). Reverse transcription-quantitative polymerase chain reaction (RT-qPCR) was performed in a total volume of 20 μL containing 1 μL of cDNA template, 0.2 μM primers, and 10 μL of TB Green Premix Ex Taq II (Takara, Kusatsu, Shiga, Japan). RT-qPCR was conducted using a CFX96TM Real-time PCR system (Bio-Rad, Hercules, CA, USA) with the following program: 95°C for 5 min, followed by 40 cycles at 95°C for 10 s and 65°C for 30 s. Actin (AB181991) was used as an internal control. The primers used in this experiment are listed in Table S1.

Functional analysis of DEGs

All expressed genes under both control and stress conditions were subjected to Gene Set Enrichment Analysis (GSEA) using the GSEA software (Subramanian et al., 2005). The gene matrix transposed file format (.GMT) of wheat was downloaded from g:Profiler (https://biit.cs.ut.ee/gprofiler/gost), a web server for functional enrichment analysis and gene list conversion (*Raudvere et al*., *2019*). The enrichment score of each gene set was calculated using the full ranking, and the normalized enrichment score (NES) was determined for each gene set. The GSEA results, including rank, expression, and class files, were visualized as a network using Enrichment Map (*Merico et al*., *2010*). For Kyoto Encyclopedia of Genes and Genome (KEGG) pathway enrichment analysis, the KEGG Orthology Database in KOBAS-i was used to predict the putative pathways of DEGs (*Bu et al*., *2021*). The plant transcription factor data were obtained from the Plant Transcription Factor Database (PlantTFDB) (*Tian et al*., *2020*). Protein Basic Local Alignment Search Tool (BLASTP) was used on the peptide sequences of the DEGs, based on the local transcription factor database obtained from PlantTFDB, with an E-value threshold of 1×10^{-1} and sequence identity of >80%. Mev software (http://sourceforge.net/projects/mev-tm4/files/mev-tm4/) was used for k-means clustering of DEGs identified from the GSEA, KEGG pathway, and transcription factor analyses. The results of the GSEA and KEGG pathway analysis were generated using an R script and the ggplot2 R package. Additionally, MapMan (*Sreenivasulu et al*., *2008*) was used to identify the pathways of stage-specific genes.

Enzyme activities assays

The crude enzyme was extracted from 100 mg of wheat leaves using a protein extraction buffer containing 50 mM potassium phosphate buffer (pH 7.5). The activities of catalase (CAT), peroxidase (POD), and superoxide dismutase (SOD) and total antioxidant activity (TAC) were measured using commercially available assay kits. Specifically, CAT activity was determined using a catalase microplate assay kit (kit number: MBS8243260; MyBiosource, Inc., San Diego,

CA, USA), POD activity was measured using a POD assay kit (kit number: KTB1150; Abbkine, Inc., Wuhan, China), and SOD activity was estimated using a total SOD activity assay kit (WST-1 method) (kit number: MBS2540402; MyBiosource, Inc., San Diego, CA, USA). TAC was assessed using a TAC assay kit (kit number: MAK187; Sigma-Aldrich, St. Louis, MO, USA). The preparation of the reaction mixture and the calculations for each measurement were performed as described in the respective protocol books provided with each assay kit.

Results

Characteristics of the salt-tolerant colored wheat mutant induced via gamma irradiation

Throughout the mutation breeding process, detailed records of agricultural traits, including the flowering time, plant height, and yield, were meticulously collected for the mutant lines. These data allowed for a comprehensive assessment of the phenotypic characteristics of the lines. Evidence supporting the stable phenotype of the mutant lines is provided in Fig. S1, which also presents the field performance of PL1 and PL6. Additionally, the difference in grain color between the colored wheat lines used in this study and common wheat lines cultivated in Korea is illustrated in Fig. S2. Through preliminary salt-tolerance screening, PL6 was selected as the gamma ray-derived mutant line that exhibited favorable salt-tolerance characteristics (Fig.S3). To assess the growth response of the control line (PL1) and PL6 under varying salt concentrations, the seeds were treated with NaCl solutions of 50, 100, 150, 200, 250, 300, and 500 mM, along with distilled water as the control (*Choudhary et al*., *2021*). Overall, high salt concentrations negatively affected seed germination and seedling growth (Figs. 1A and 1B). The germination percentage and seedling growth were reduced with increasing salt concentration in both PL1 and PL6 (Table S2). However, PL6 demonstrated higher germination percentages, particularly at the maximum NaCl concentration, exceeding those of PL1. Remarkably, a maximum increase of 20% in germination was observed for PL6 following treatment with 250 mM NaCl. Moreover, PL6 consistently outperformed PL1 in terms of seedling growth under all salt treatment conditions, as evidenced by its longer shoot and root lengths (Figs. 1C and 1D). The comprehensive data strongly indicates that the gamma ray-derived mutant PL6 exhibits higher resistance to salt stress than PL1.

Assessment of Na^+, K^+, and chlorophyll contents under salt stress conditions

Prior to treatment, PL6 had a higher Na^+ ion content than PL1 (Fig. 2A). However, with increasing time of exposure to salt stress, the Na^+ ion content markedly increased in both PL1 and PL6. Notably, the rate of increase in Na^+ ion content was lower in PL6 than in PL1. Conversely, the K^+ ion content steadily decreased with salt treatment in both PL1 and PL6 (Fig. 2B). To further analyze the ion contents, we calculated the relative ratios of K^+ and Na^+ ions in PL1 and PL6, considering their respective contents under control conditions (Figs. 2C and 2D). In PL1, the Na^+ ion content increased significantly by 47 times from the baseline (0 h) to 48 h following salt treatment. In contrast, PL6 exhibited a milder increase in Na^+ ion content, approximately 20 times higher at 48 h after salt stress. Consequently, the relative Na^+ content was more profoundly affected by salt stress in PL1 than in PL6. Interestingly, the chlorophyll concentrations of both PL1 and PL6 remained relatively stable under salt stress (Fig. 2E), indicating that they were not significantly affected by the imposed salinity conditions.

DEGs during salt stress

After treatment with 150 mM NaCl, leaves were harvested from PL1 and PL6 at 0, 3, 24, and 48 h and subjected to RNA sequencing. Following quality evaluation and trimming, an average of 38.1 million trimmed reads and over 22.1 billion bases were generated from each sample under both control and salt stress conditions. The average percentage of Q20 and Q30 bases was found to be 98.4% and 95.5%, respectively, indicating high sequencing quality. Moreover, >96% of the sequenced data exhibited an average mapping rate of 96.16%, successfully aligning to the IWGSC wheat reference sequence (Table S3). During data analysis, a total of 4,017 DEGs were identified with a p-value of <0.05, FDR of <0.05, and absolute fold change value of >2 (Fig. 3A and Table S4). Specifically, in PL1, 872, 1,588, and 1,080 DEGs were identified at 3, 24, and 48 hours after salt treatment, respectively, in comparison to the untreated condition (0h) (Fig. 3B). Similarly, for PL6, the number of DEGs was 566, 1,248, and 1,810 at 3, 24, and 48 hours after salt treatment, respectively (Fig. 3C). These results highlight the dynamic gene expression changes in PL1 and PL6 under salt stress at different timepoints, contributing to a better understanding of the underlying molecular responses to salt stress in these wheat lines.

Functional analysis of the DEGs during salt stress

Overall, 33 GO terms were identified for each treatment condition (Fig. 3D and Table S5). Notably, several gene sets, including defense response (GO: 0006952), glutathione metabolic process (GO: 0006749), peroxidase activity (GO: 0004601), ROS metabolic process (GO: 0072593), response to biotic stimulus (GO: 0009607), and response to stress (GO: 0006950), were positively correlated with salt stress and PL6, exhibiting a positive NES (Fig. 3D). To visualize the results, all the gene sets from the GSEA were organized into four networks using Enrichment Map (*Merico et al*., *2010*) (Figs. 4A–4E). The expression patterns of each network in Figs. 4A–4E for PL1 and PL6 were clustered by expressed patterns (Figs. 4F–4J, respectively). The K-means clustering algorithm in the Mev software was used to identify the clusters of DEGs in each GO term under control and salt stress conditions based on their expression patterns. Most of the expression patterns from the identified clusters did not differ between the control and salt stress conditions. Three clusters that demonstrated different expression patterns for PL1 and PL6, especially those upregulated in PL6, were selected and marked in red boxes in Figs. 4F, 4G, and 4I, and a heatmap of the genes from these clusters was generated (Fig. 4K). Plant hormone-related genes (*TRAESCS1B02G145800 and TRAESCS1B02G138100*), ROS-related genes (*TRAESCS1B02G059100*, *TRAESCS1B02G095800*, *TRAESCS1B02G096200*, *TRAESCS1B02G096900*, and *TRAESCS1B02G115900*), and stress-response genes (*TRAESCS5D02G492900*, *TRAESCS1A02G009900*, *TRAESCS1B02G023000*, and *TRAESCS2A02G037400*) were highly expressed in PL6 under salt stress conditions. Furthermore, six genes related to chromatin remodeling (*TRAESCS1B02G048900*, *TRAESCS1B02G049100*, *TRAESCS1D02G286700*, *TRAESCS1B02G149000*, and *TRAESCS7D02G246600*) showed high expression patterns in PL6 under salt stress conditions [Table 1]. A high number of transcriptomes of MADS-box transcription factors (*TRAESCS4A02G002600*, and *TRAESCS6D02G293200*) were also detected in PL6 under salt stress. An auxin-responsive protein (*TRAESCS1B02G138100*) and probable histone H2A variant 3 (*TRAESCS7D02G246600*) were also found in cluster 4 [Table 1].

In the case of the differences in the KEGG pathways between PL1 and PL6 under salt stress conditions, the rich factor of "Biosynthesis of secondary metabolites" in PL6 after 3 h of salt stress

was ~0.05, increasing to ~0.2 after 48 h of salt stress (Fig. 5). Likewise, the rich factors of "Flavonoid biosynthesis" were 0.17 and 0.23, after 24 and 48 h of salt stress, respectively. This was only observed in PL6 during salt stress conditions (Fig. 5 and Table S6).

In addition to GO and KEGG analysis, the role of DEGs as transcription factors was investigated. DEGs at different timepoints under salt stress in PL1 and PL6 were identified using PlantTFDB (http://planttfdb.gao-lab.org). In total, 255 genes were identified with an e-value threshold of 1×10^{-1} and a sequence identity of >80% and further selected to compare the expression patterns between PL1 and PL6 under salt stress conditions. The most abundant type of transcription factor was the ethylene-response factor (ERF) protein family, followed by the basic helix-loop-helix (bHLH) protein family; heat shock transcription factor protein family; myeloblastosis (MYB)-related protein family; and Nam, ATAF, and CUC (NAC) protein family (Fig. 6A). Moreover, 255 putative transcription factors were grouped by expression pattern into six clusters and an unclassified group (Fig. 6B). Overall, 72, 44, and 35 DEGs were annotated by the ERF, bHLH, and MYB (related) protein families, respectively. These three transcription factors accounted for 59% of the total number of transcription factors. The expression patterns of DEGs in clusters 2 and 6 (marked with red boxes in Fig. 6B) were selected and expressed in heatmaps (Fig. 6C) to display differences in the expression patterns of DEGs between PL1 and PL6 under salt stress conditions (Table S7). Notably, PL6 exhibited higher expression of specific transcription factors under salt stress conditions than PL1, as displayed in the heatmap (Fig. 6C).

Lastly, 22 protein kinase genes were identified with significant expression patterns at different timepoints, including two calcineurin B-like (CBL)-interacting protein kinases and one mitogen-activated protein kinase (MAPK) with more than two-fold changes in PL6 under salt stress (Table 2). Additionally, 70 differentially expressed salt stress-responsive genes involved in regulating the circadian clock system, cytoskeleton organization, and cell wall organization were identified using MapMan, with 15 of them showing more than a two-fold change in PL6 (Table 3).

Enzyme activities assays

To investigate the differences in enzyme activities between PL1 and PL6 under salt stress conditions, we measured CAT, POD, and SOD activities and TAC (Fig. 7). Upon subjecting both wheat lines to salt stress, we observed distinct patterns in enzyme activities. In PL6, CAT and POD activities significantly increased after 24 and 48 h of exposure to salt stress (Fig. 7A and B). Conversely, in PL1, SOD activity slightly decreased after 24 and 48 h exposure to salt stress (Fig. 7C). Furthermore, the TAC in PL1 was not significantly changed by salt stress (Fig. 7D). Conversely, in PL6, the TAC notably increased after 24 and 48 h of exposure to salt stress. This increase in TAC suggests that PL6 has a higher capacity to counteract oxidative stress and maintain cellular redox balance than PL1, contributing to its enhanced salinity tolerance.

Validation of the DEG results using reverse transcription-quantitative polymerase chain reaction

Supporting the DEG results, 12 genes from the three aforementioned clusters from PL1 and PL6 were selected for RT-qPCR (Fig. 8). All the selected genes were more highly expressed in PL6 than in PL1. *peroxidase 2* (*TRAESCS1B02G095800)*, *nitrate transporter* (*TRAESCS1B02G038700*), *auxin-responsive protein* (*TRAESCS1B02G138100)*, and *replication*

protein A (*TRAESCS1B02G102200)* transcripts in PL6 were highly expressed at 48 h following salt treatment (Fig. 8A). *Nuclear transport factor 2- like protein* (*TRAESCS2A02G046200)*, *histone H2A* (*TRAESCS1B02G048900)*, *integral membrane protein* (*TRAESCS1B02G071800)*, and *histone H2A variant 3 (TRAESCS7D02G246600)* transcripts in PL6 continuously decreased at 24 h and peaked at 48 h following salt treatment (Fig. 8B). *Argonaute 1C-like isoform X2 (TRAESCS6B02G466700)*, *MADS-box (TRAESCS6B02G017900),* and *aspartokinase 1 (TRAESCS5D02G537600)* transcripts in PL6 peaked at 3 h, and all gradually decreased, except for *ribosome biogenesis protein NOP53* (*TRAESCS1B02G105100)* (Fig. 8C). These results are consistent with those of RNA sequencing (RNA-seq).

Discussion

This study revealed that salinity stress had negative effects on germination and plant growth during the developmental process. Na^+ is considered a nonessential element in plants (*Nieves-Cordones et al*., 2016); however, excessive accumulation of Na^+ can have detrimental effects on plants, including disrupting cellular homeostasis, inducing oxidative stress, and suppressing growth (*Munns & Tester*, *2008*; *Craig Plett*, *2010*). In this study, PL6 consistently showed higher germination rates and better seedling growth under salt stress than PL1. The differences in K+ and Na+ contents between PL1 and PL6 supported these observations, highlighting PL6's superior performance under salt treatment conditions. Previous research on different rice genotypes demonstrated varying germination rates and nutrient survival under salt stress, which was associated with differences in ion concentration and homeostasis (*Craig Plett*, *2010*). Similarly, reduction of Na^+ accumulation and maintenance of K^+ accumulation in the shoots have been shown to play an important role in salinity tolerance in barley and maize (*Tester & Davenport*, *2003*; *Chen et al*., *2007*).

Genome-wide transcriptomic analysis has emerged as a powerful tool to investigate stress-tolerant genes, gene families, and related mechanisms in plants (*Peng et al*., *2014*; *Li et al*., *2016*). In this study, we observed a significant difference in the salinity response between PL1 and PL6 and identified distinct expression patterns of DEGs between the two lines. Although a higher number of DEGs was found in PL6 compared with PL1, it is important to note that the majority of these DEGs exhibited similar expression patterns in both PL1 and PL6 under salt stress conditions. This could be because PL6 was generated through a mutation of PL1 via gamma irradiation, leading to the sharing of numerous genomes between them. Nonetheless, despite the similar expression patterns, clear phenotypic differences were observed, including variations in germination rate, shoot and root growth, and ion concentrations (Na^+ and K^+). Thus, our genome-wide transcriptional analysis allowed us to identify the DEGs responsible for the differential responses of PL1 and PL6 under salt stress conditions.

Salt stress not only induces osmotic stress but also leads to ionic imbalance, resulting in ion toxicity and, ultimately, the production of ROS (*Julkowska & Testerink*, *2015*). In our study, PL1 (as the wild-type line) exhibited a dark-purple seed coat and had high levels of anthocyanin, phenolic

compounds, and antioxidant activities (*Hong et al*., *2019*). Similarly, PL6, which was generated by irradiating PL1 with 200 Gy of gamma rays, also displayed a dark-purple seed coat.

As shown in Figure 3D, GSEA revealed several GO terms that were positively correlated with salt stress, including defense response (GO: 0006952), glutathione metabolic process (GO: 0006749), peroxidase activity (GO: 0004601), ROS metabolic process (GO: 0072593), response to biotic stimulus (GO: 0009607), and response to stress (GO:0006950). Among these terms, three were specifically related to antioxidant activity: glutathione metabolic process (GO: 0006749), peroxidase activity (GO: 0004601), and ROS metabolic process (GO: 0072593). These antioxidant-related GO terms are crucial protective mechanisms against salinity stress in plants. Interestingly, we observed that DEGs related to antioxidants were specifically upregulated in PL6 48 h after salt stress, despite both PL1 and PL6 having colored seed coats. This suggests that these DEGs may positively contribute to salt stress tolerance, leading to more vigorous shoot and root growth in PL6 than that in PL1. In addition to the gene expression analysis, the measurement of antioxidant enzyme activities further supports the higher antioxidant capacity in PL6 than in PL1 under salt stress conditions. CAT and POD activities were significantly increased at 24 and 48 h after salt stress exposure in PL6 (Fig. 7A and B), indicating efficient ROS-scavenging ability and peroxide detoxification, which help protect the cells from oxidative damage during salt stress. Conversely, in PL1, SOD activity slightly decreased at 24 and 48 h post-salt stress (Fig. 7C), suggesting a limited ability to efficiently neutralize superoxide radicals, potentially leading to ROS accumulation and oxidative stress in PL1 under salt stress conditions. Overall, these findings not only provide insights into the DEGs related to antioxidant activity but also highlight the distinctive enzymatic responses to salt stress in PL1 and PL6. The increases in CAT and POD activities and TAC in PL6 might play crucial roles in its superior ability to manage salt-induced oxidative stress compared with the wild-type PL1. The combination of gene expression analysis and antioxidant enzyme activity measurements sheds light on the activation of specific antioxidant pathways in PL6, providing a comprehensive understanding of its enhanced salinity stress response.

Phytohormones, such as abscisic acid (ABA) and auxins (indole acetic acid [IAA] and indole-3-butyric acid), play crucial roles in plant responses to environmental stresses, including salinity. ABA is a key signaling molecule involved in the adaptation to salt stress in various crop plants, such as tobacco, alfalfa, common bean, and potato (*Sah et al*., *2016*). Meanwhile, IAA contributes to maintaining growth in salt-resistant maize genotypes by regulating shoot turgor and growth through significant increases in shoot sap osmolality (*Zolman & Bartel*, *2004*; *De Costa et al*., *2007*). In this study, we observed increased transcription levels of TRAESCS1B02G145800 (ABA receptor PYL8) and TRAESCS1B02G138100 (auxin-responsive protein IAA15) in PL6 under salt stress conditions (Table 1). Additionally, salinity-induced osmotic stress leads to the overproduction of ROS and oxidative damage to plant cells. To counteract this, the antioxidant defense system in plants is activated to detoxify ROS and maintain redox homeostasis (*Hasanuzzaman et al*., *2021*). Accordingly, we found that plant hormone-related genes, including dehydroascorbate reductase and peroxidase genes, were upregulated in PL6 under salt stress to

protect against ROS-induced damage and maintain cellular redox balance (Table 1). The increased expression of ROS-related genes in PL6 suggests that this mutant line may exhibit an altered response to salt stress-induced oxidative stress.

In addition to hormone-related responses, transcriptional regulation through histone modification and chromatin remodeling plays a pivotal role in plant responses to salt stress. In this study, we observed an increase in the transcription levels of INO80 complex subunit D (TRAESCS1B02G149000) in PL6 under salt stress conditions. The INO80 chromatin remodeling complex is responsible for evicting the histone variant H2A.Z in eukaryotic cells (*Alatwi & Downs*, *2015*). Studies in *Arabidopsis* have demonstrated that under salt stress, the INO80 complex induces the eviction of H2A.Z-containing nucleosomes from the AtMYB44 promoter region, leading to increased accumulation of AtMYB44 transcripts and thus promoting salt stress tolerance (*Nguyen & Cheong*, *2018*). However, the specific target gene and position of the histone variant H2A.Z evicted by the INO80 complex in wheat remain unclear. Further investigations are required to identify the precise position of H2A.Z evicted by the INO80 complex and clarify the factors influencing the differential responses of PL1 and PL6 to salinity stress.

Moreover, investigation of the MADS-box family members contributes to our understanding of the differential responses of PL1 and PL6 to salinity stress. MADS-box transcription factors are known to regulate flowering development (*Lee & Lee*, *2010*; *Callens et al*., *2018*). *Wu et al*. (*2020*) reported that overexpression of *OsMADS25* in rice and *Arabidopsis* resulted in improved salinity tolerance compared with that in the wild-type. Conversely, the MADS-box transcription factor *AGL16* was identified as a negative regulator of stress responses in *Arabidopsis* (*Zhao et al*., *2021*). In this study, we observed increased transcription levels of two MADS-box transcription factors (TRAESCS4A02G002600 and TRAESCS6D02G293200) in PL6 mutant plants under salt stress conditions, suggesting their potential roles in salt tolerance and growth response. These findings provide valuable insights into the molecular mechanisms underlying the differential responses of PL1 and PL6 to salinity.

Furthermore, although GO terms related to photosynthesis were detected via GSEA and network analysis (Figs. 3D and 4B), no significant differences were observed in the gene expression patterns between PL1 and PL6. This finding is consistent with the data on chlorophyll concentration (Fig. 2E), which did not show significant variation between PL1 and PL6 during the duration of salt stress exposure. In our previous study, we observed that the total anthocyanin concentrations in wheat mutant lines (used in this study) were significantly higher than those in wild-type lines, resulting in higher antioxidant activity in the mutants compared with the wild-type (*Hong et al*., *2019*). In the present study, the enriched factors “Biosynthesis of secondary metabolites” and “Flavonoid biosynthesis” increased following salt stress treatment (Fig. 5). This suggests that the antioxidant activities of PL6 under salt stress conditions might be influenced by these pathways, which include genes associated with GO terms such as glutathione metabolic process (GO: 0006749), peroxidase activity (GO: 0004601), and ROS metabolic process (GO: 0072593) (Fig. 3D).

As shown in Fig. 4D, several DEGs were mapped to GO terms related to gene expression regulation (GO: 001046), DNA binding transcription factor activity (GO: 0003700), and transcription regulator activity (GO: 0140110). To elucidate the molecular mechanism of salt stress response at the cellular level, we analyzed putative transcription factors and selected those with differential expression patterns in PL6 under salt stress conditions. Among them, the ERF family protein emerged as an important family of transcription factors in plants, regulating various developmental processes (*Nakano*, *2006*), including their response to salt stress (*Cheng et al*., *2013*; *Li et al*., *2020b*; *Trujillo et al*., *2008*). Additionally, studies have revealed the significance of the bHLH and MYB gene families in the response to salt stress in plants (*Yang et al*., *2021*; *Li et al*., *2020a*; *Jiang et al*., *2009*; *Kim et al*., *2013*; *Seo et al*., *2012*). The putative transcription factors shown in Fig. 6 can be further analyzed for their functions to better understand the molecular mechanisms of salt response. Flavonoid biosynthesis has been extensively studied and is predominantly regulated at the transcriptional level by the MYB–bHLH-WD40 complex in various plant species, such as rice, *Arabidopsis*, Mimulus, apples, and maize (*Tohge et al*., *2017*; *An et al*., *2020*; *Yuan et al*., *2014*; *Zheng et al*., *2019*; *Baudry et al*., *2006*). In this study, several bHLH and MYB gene families were identified as putative transcription factors, likely influenced by the seed colors of PL1 (wild-type) and PL6 (mutant line) used in the experiment. Consequently, based on the heat map in Fig. 6, the bHLH and MYB gene families exhibiting different expression patterns between PL1 and PL6 were considered differentially expressed transcription factors under salt stress conditions.

Moreover, protein kinases play a vital role in regulating plant responses to salt stress. *Singh et al*. (*2018*) investigated the expression levels of protein kinase genes in response to salt stress in rice plants. They found that two CBL-interacting protein kinases and one MAPK showed more than a two-fold change in PL6 rice lines under salt stress. Similarly, *Xiong et al*. (*2003*) highlighted the significance of the MAPK gene *OsMPK5* in regulating the salt stress response in rice plants. Apart from MAPKs, other types of protein kinases have also been implicated in salt stress response. For instance, the protein kinase OsSOS2 is involved in regulating salt tolerance in rice plants by activating the SOS pathway (*Kumar et al*., *2022*). Another study reported that the receptor-like kinase OsWAK35 plays a role in regulating salt stress response in rice plants by activating the MAPK pathway (*Zhang et al*., *2005*). These findings underscore the importance of protein kinases in the regulation of plant responses to salt stress and suggest that different types of protein kinases play specific roles in these processes.

In the present study, we identified 15 DEGs with more than a two-fold change, among which one, five, and nine genes were involved in the circadian clock system, cytoskeleton organization, and cell wall organization, respectively (Table 3). These processes play crucial roles in plant stress response and are important components of how plants adapt to challenging environments. The circadian clock system has been found to be essential in regulating the plant's response to salt stress. *Xu et al*. (*2022*) conducted a study on *Arabidopsis* plants and demonstrated that the circadian clock system is involved in the modulation of salt stress responses. They observed altered

expression levels of circadian clock genes under salt stress conditions and further noted that the disruption of the circadian clock system resulted in reduced salt tolerance in the plants. Likewise, the cytoskeleton organization is also critical for regulating plant responses to salt stress. For instance, in rice plants, the actin cytoskeleton has been shown to play a role in regulating the response to salt stress, ion homeostasis, and ROS scavenging (*Chun et al*., *2021*). Disruption of the actin filaments in rice plants led to reduced salt tolerance, indicating the importance of the cytoskeleton in coping with salt-induced stress. Moreover, the cell wall organization is a vital aspect of the response of maize to salt stress. A study on maize revealed that the expression of genes related to the cell wall was altered under salt stress conditions, and modification of the cell wall composition contributed to increased salt tolerance in the plants (*Oliveira et al*., *2020*). These findings highlight the significance of the cell wall in mediating the plant's ability to withstand salt stress.

The primary focus of this study was to investigate the molecular mechanisms underlying salinity stress responses in the colored wheat mutant PL6 through transcriptomic profiling of leaf tissues. However, considering the crucial role of roots in nutrient and mineral absorption, examining the variations in Na^+ and K^+ levels in root tissues could provide valuable insights into tissue-specific ion absorption and accumulation mechanisms in PL6. Furthermore, conducting a comprehensive analysis of DEGs in root tissues could reveal novel genes and pathways associated with salt stress responses that significantly contribute to the enhanced tolerance observed in PL6. Further research incorporating histological analyses of root tissues and transcriptomic profiling of roots would be instrumental in unraveling the genetic basis and tissue-level adaptations responsible for the superior salt stress response and tolerance of PL6.

In summary, this investigation of the effects of salinity stress on two wheat lines, namely PL1 (wild-type) and PL6 (mutant line generated through gamma irradiation of PL1), revealed that salt stress negatively affected germination and plant growth in both lines. However, PL6 demonstrated greater tolerance to salinity stress than PL1, indicating that the mutant line has acquired mechanisms to more effectively mitigate salt stress-induced damage. The differences in ion concentrations observed in PL6, including lower Na^+ levels and higher K^+ levels, suggest better ion homeostasis in this line, contributing to its enhanced salt stress tolerance. Our genome-wide transcriptomic analysis provided insights into the differential expression patterns of genes between PL1 and PL6 under salt stress conditions, leading to the observed phenotypic differences. Several GO terms related to defense responses, glutathione metabolism, peroxidase activity, and ROS metabolic processes were positively correlated with salt stress, highlighting the importance of antioxidant activities in salt tolerance. The specific upregulation of DEGs related to antioxidants in PL6, despite both lines having colored seed coats, suggests that these DEGs play critical roles in enhancing salt stress tolerance and promoting vigorous shoot and root growth. Additionally, hormone-related genes, transcription factors, and protein kinases displayed differential expression, indicating their involvement in the differential salt stress responses between PL1 and PL6. The enrichment of pathways related to flavonoid biosynthesis and secondary metabolite biosynthesis

in PL6 further suggests their contribution to the enhanced antioxidant activities observed in this line. It is important to acknowledge that the mechanisms underlying salt stress resistance in plants are highly complex and not easily discernible. The interplay of various genetic, physiological, and biochemical factors contributes to the overall response to salinity stress, making it challenging to draw straightforward conclusions. Nevertheless, understanding these intricate mechanisms is crucial for developing stress-tolerant crop varieties and improving agricultural practices. By gaining insights into the genes and pathways responsible for salt stress tolerance, researchers can design targeted breeding programs to develop salt-resistant crop varieties, thereby enhancing global food production and addressing food security challenges.

Conclusions

Salt stress in agriculture has significant impact on crop productivity, leading to reduced yields and economic losses. One Approach to address these issues in the breeding of salt tolerant crop varieties. Through mutation breeding, the selected PL6 was found to have resistance to salt stress compared to the original variety, PL1, as determined by germination rate, plant growth, and Na^+/K^+ ion levels. This study could provide valuable information on the differential responses of the wheat lines PL1 and PL6 to salinity stress. The identification of various genes and pathways associated with salt stress tolerance in PL6 offers promising avenues for further research and potential applications in crop improvement. As we continue to unravel the intricate network of stress-tolerant mechanisms in plants, we move closer to the goal of developing resilient and productive agricultural systems to ensure food security in the face of environmental challenges. Because PL6 was developed through mutation breeding, it can be used as a breeding parent or genetic material. Mutation breeding is a technique used to increase genetic diversity by inducing mutations through exposure to radiation, chemical agents, or other mutagenic factors, and it is widely used for rapid and effective plant improvement. Because of mutagenesis in PL6, it possesses distinct characteristics from its original parent PL1 and exhibits higher tolerance to environmental stresses, displaying different responses from PL1. The traits resulting from this mutation are stably inherited genetically, making PL6 a valuable genetic resource that can be used as a breeding parent or crossed with other genetic materials to develop new genotypes. In conclusion, the remarkable salt stress tolerance exhibited by PL6, a result of mutation breeding, positions it as a crucial genetic resource for enhancing agricultural productivity and ensuring food security. The unique characteristics acquired through mutagenesis make PL6 a valuable breeding parent or genetic material, showing higher tolerance to environmental stresses compared to its parent, PL1. The stability in the genetic inheritance of these traits underscores the potential of PL6 in contributing significantly to the development of new plant varieties suited for resilience in challenging agricultural conditions. Emphasizing salt stress tolerance, PL6 stands as a guide for future research and development endeavors, promising more effective utilization of plant genetic resources and continued contributions to the advancement of strong and adaptive crop varieties.

References

Al-Ashkar I, Alderfasi A, El-Hendawy S, Al-Suhaibani N, El-Kafafi S, Seleiman M. 2019. Detecting salt tolerance in doubled haploid wheat lines. *Agronomy* **9(4)**:211 DOI 10.3390/agronomy9040211.

Alatwi HE, Downs JA. 2015. Removal of H2A.Z by INO80 promotes homologous recombination. *EMBO Reports* **16(8)**:986–994 DOI 10.15252/embr.201540330.

Amirbakhtiar N, Ismaili A, Ghaffari MR, Nazarian Firouzabadi F, Shobbar ZS. 2019. Transcriptome response of roots to salt stress in a salinity-tolerant bread wheat cultivar. *PLOS ONE* **14(3)**:e0213305 DOI 10.1371/journal.pone.0213305.

An JP, Wang XF, Zhang XW, Xu HF, Bi SQ, You CX, Hao YJ. 2020. An apple Myb transcription factor regulates cold tolerance and anthocyanin accumulation and undergoes Miel1-mediated degradation. *Plant Biotechnology Journal* **18(2)**:337–353 DOI 10.1111/pbi.13201.

Anders S, Pyl PT, Huber W. 2015. Htseq—A python framework to work with high-throughput sequencing data. *Bioinformatics* **31(2)**: 166–169 DOI 10.1093/bioinformatics/btu638.

Asif MA, Schilling RK, Tilbrook J, Brien C, Dowling K, Rabie H, Short L, et al. 2018. Mapping of novel salt tolerance QTL in an Excalibur × Kukri doubled haploid wheat population. TAG. *Theoretical and Applied Genetics* **131**:2179–2196 DOI 10.1007/s00122-018-3146-y.

Baudry A, Caboche M, Lepiniec L. 2006. Tt8 controls its own expression in a feedback regulation involving Ttg1 and homologous Myb and bHLH factors, allowing a strong and cell-specific accumulation of flavonoids in Arabidopsis thaliana. *The Plant Journal* **46(5)**:768–779 DOI 10.1111/j.1365-313X.2006.02733.x.

Callens C, Tucker MR, Zhang D, Wilson ZA. 2018. Dissecting the role of MADS-box genes in monocot floral development and diversity. *Journal of Experimental Botany* **69(10)**: 2435–2459 DOI 10.1093/jxb/ery086.

Chele KH, Tinte MM, Piater LA, Dubery IA, Tugizimana F. 2021. Soil salinity, a serious environmental issue and plant responses: A metabolomics perspective. *Metabolites* **11(11)**:724 DOI 10.3390/metabo11110724.

Chen Z, Pottosin II, Cuin TA, Fuglsang AT, Tester M, Jha D, Zepeda-Jazo I, Zhou M, Palmgren MG, Newman IA, Shabala S. 2007. Root plasma membrane transporters controlling K+/Na+ homeostasis in salt-stressed barley. *Plant Physiology* **145(4)**:1714–1725 DOI 10.1104/pp.107.110262.

Cheng MC, Liao PM, Kuo WW, Lin TP. 2013. The Arabidopsis ethylene response Factor1 regulates abiotic stress-responsive gene expression by binding to different cis-acting elements in response to different stress signals. *Plant Physiology* **162(3)**:1566–1582 DOI 10.1104/pp.113.221911.

Choudhary A, Kaur N, Sharma A, Kumar A. 2021. Evaluation and screening of elite wheat germplasm for salinity stress at the seedling phase. *Physiologia Plantarum* **173(4)**:2207–2215 DOI 10.1111/ppl.13571.

Chun HJ, Baek D, Jin BJ, Cho HM, Park MS, Lee SH, Lim LH, Cha YJ, Bae DW, Kim ST, Yun DJ, Kim MC. 2021. Microtubule dynamics plays a vital role in plant adaptation and tolerance to salt stress. *International Journal of Molecular Sciences* **22(11)**:5957 DOI 10.3390/ijms22115957.

Colmer T D, Flowers, T J, Munns R. 2006. Use of wild relatives to improve salt tolerance in wheat. *Journal of Experimental Botany* **57(5)**:1059–1078 DOI 10.1093/jxb/erj124.

Craig Plett D, Møller IS. 2010. Na(+) transport in glycophytic plants: What we know and would like to know. *Plant, Cell & Environment* **33(4)**:612–626 DOI 10.1111/j.1365-3040.2009.02086.x.

Assaha DVM, Ueda A, Saneoka H, Al-Yahyai R, Yaish MW. 2017. The role of Na+ and K+ transporters in salt stress adaptation in glycophytes. *Frontiers in Physiology* **8**:509 DOI 10.3389/fphys.2017.00509.

De Costa W, Zörb C, Hartung W, Schubert S. 2007. Salt resistance is determined by osmotic adjustment and abscisic acid in newly developed maize hybrids in the first phase of salt stress. *Physiologia Plantarum* **131(2)**:311–321 DOI 10.1111/j.1399-3054.2007.00962.x.

Deinlein U, Stephan AB, Horie T, Luo W, Xu G, Schroeder J I. 2014. Plant salt-tolerance mechanisms. *Trends in Plant Science* **19(6)**:371–379 DOI10.1016/j.tplants.2014.02.001.

El-Hendawy S. E, Hassan WM, Al-Suhaibani NA, Refay Y, Abdella KA. 2017. Comparative performance of multivariable agro-physiological parameters for detecting salt tolerance of wheat cultivars under simulated saline field growing conditions. *Frontiers in Plant Science* **8**:435 DOI 10.3389/fpls.2017.00435.

El-Hendawy S, Elshafei A, Al-Suhaibani N, Alotabi M, Hassan W, Dewir YH. Abdella K. 2019. Assessment of the salt tolerance of wheat genotypes during the germination stage based on germination ability parameters and associated SSR markers. *Journal of Plant Interactions* **14(1)**:151–163 DOI 10.1080/17429145.2019.1603406.

EL Sabagh A, Islam MS, Skalicky M, Ali Raza M, Singh K, Anwar Hossain M, et al. 2021. Salinity stress in wheat (*Triticum aestivum* L.) in the changing climate: Adaptation and management strategies. *Frontiers in Agronomy* **3**:661932 DOI 10.3389/fagro.2021.661932.

Genc Y, Taylor J, Lyons G. Li Y, Cheong J, Appelbee M, Oldach K, Sutton T. 2019. Bread wheat with high salinity and sodicity tolerance. *Frontiers in Plant Science* **10**:1280 DOI 10.3389/fpls.2019.01280.

Hanin M, Ebel C, Ngom M, Laplaze L, Masmoudi K. 2016. New insights on plant salt tolerance mechanisms and their potential use for breeding. *Frontiers in Plant Science* **7**:1787 DOI 10.3389/fpls.2016.01787.

Hasanuzzaman M, Alam MM., Rahman A, Hasanuzzaman M, Nahar K, Fujita M. 2014. Exogenous proline and glycine betaine mediated upregulation of antioxidant defense and glyoxalase systems provides better protection against salt-induced oxidative stress in two rice

(*Oryza sativa* L.) varieties. *BioMed Research International* **2014**: Article ID 757219 DOI 10.1155/2014/757219.

Hasanuzzaman M, Raihan MRH, Masud AAC, Rahman K, Nowroz F, Rahman M, Nahar K, Fujita M. 2021. Regulation of reactive oxygen species and antioxidant defense in plants under salinity. *International Journal of Molecular Sciences* **22(17)**:9326 DOI 10.3390/ijms22179326.

Hong MJ, Kim DY, Nam BM, Ahn JW, Kwon SJ, Seo YW, Kim JB. 2019. Characterization of novel mutants of hexaploid wheat (Triticum aestivum L.) with various depths of purple grain color and antioxidant capacity. *Journal of the Science of Food and Agriculture* **99(1)**:55–63 DOI 10.1002/jsfa.9141.

Horie T, Hause, F, Schroeder JI. 2009. HKT transporter-mediated salinity resistance mechanisms in *Arabidopsis* and monocot crop plants. *Trends in Plant Science* **14(12)**:660–668 DOI 10.1016/j.tplants.2009.08.009.

Huang S, Spielmeyer W, Lagudah ES, Munns, R. 2008. Comparative mapping of HKT genes in wheat, barley, and rice, key determinants of Na+ transport, and salt tolerance. Journal of Experimental Botany **59(4)**:927–937. DOI 10.1093/jxb/ern033.

Hussain N, Ghaffar A, Zafar ZU, Javed M, Shah KH, Noreen S, Manzoor H, Iqbal M, Hassan IFZ, Bano H, Gul HS, Aamir M, Khalid A, Sohail Y, Ashraf M, Athar H. U. R. 2021. Identification of novel source of salt tolerance in local bread wheat germplasm using morpho-physiological and biochemical attributes. *Scientific Reports* **11**:10854. DOI 10.1038/s41598-021-90280-w.

Ismail AM, Horie T. 2017. Genomics, physiology, and molecular breeding approaches for improving salt tolerance. *Annual Review of Plant Biology* **68**:405–434. DOI 10.1146/annurev-arplant-042916-040936.

Jiang Y, Yang B, Deyholos MK. 2009. Functional characterization of the *Arabidopsis* bHLH92 transcription factor in abiotic stress. *Molecular Genetics and Genomics* **282**:503–516. DOI 10.1007/s00438-009-0481-3.

Julkowska MM, Testerink C. 2015. Tuning plant signaling and growth to survive salt. *Trends in Plant Science* **20(9)**:586–594. DOI 10.1016/j.tplants.2015.06.008.

Kim D, Langmead B, Salzberg SL. 2015. HISAT: A fast spliced aligner with low memory requirements. *Nature Methods* **12**:357–360. DOI 10.1038/nmeth.3317.

Kim JH, Nguyen NH, Jeong CY, Nguyen NT, Hong SW, Lee H. 2013. Loss of the R2r3 Myb, Atmyb73, causes hyper-induction of the Sos1 and Sos3 genes in response to high salinity in *Arabidopsis*. *Journal of Plant Physiology* **170(16)**:1461–1465 DOI 10.1016/j.jplph.2013.05.011.

Kissoudis C, van de Wiel C, Visser RGF, van der Linden G. 2014. Enhancing crop resilience to combined abiotic and biotic stress through the dissection of physiological and molecular crosstalk. *Frontiers in Plant Science* **5**:207 DOI 10.3389/fpls.2014.00207.

Kumar P, Sharma PK. 2020. Soil salinity and food security in India. *Frontiers in Sustainable Food Systems* **4**:533781 DOI 10.3389/fsufs.2020.533781.

Lee J, Lee I. 2010. Regulation and function of SOC1, a flowering pathway integrator. *Journal of Experimental Botany* **61(9)**:2247–2254. DOI 10.1093/jxb/erq098.

Lichtenthaler HK. 1987. Chlorophyll and carotenoids: Pigments of photosynthetic biomembranes. *Methods in Enzymology* **148**:350–382 DOI 10.1016/0076-6879(87)48036-1.

Li H., Xu G, Yang C, Yang L, Liang Z. 2019. Genome-wide identification and expression analysis of HKT transcription factor under salt stress in nine plant species. *Ecotoxicology and Environmental Safety* **171**:435–442 DOI 10.1016/j.ecoenv.2019.01.008.

Li J, Zhu L, Hull J J, Liang S, Daniell, H Jin S, Zhang X. 2016. Transcriptome analysis reveals a comprehensive insect resistance response mechanism in cotton to infestation by the phloem feeding insect Bemisia tabaci (whitefly). *Plant Biotechnology Journal* **14(10)**:1956–1975 DOI 10.1111/pbi.12554.

Li J, Wang T, Han J, Ren Z. 2020a. Genome-wide identification and characterization of cucumber bHLH family genes and the functional characterization of CsbHLH041 in NaCl and Aba tolerance in *Arabidopsis* and cucumber. *BMC Plant Biology* **20**:1–20 DOI 10.1186/s12870-020-02440-1.

Li WY, Wang C, Shi HH, Wang B, Wang J. X, Liu YS, Ma JY, Tian SY, Zhang YW. 2020b. Genome-wide analysis of ethylene-response factor family in adzuki Bean and functional determination of Vaerf3 under saline-alkaline stress. *Plant Physiology and Biochemistry* **147**:215–222 DOI 10.1016/j.plaphy.2019.12.019.

Lloyd A, Brockman A, Aguirre L, Campbell A, Bean A, Cantero A, Gonzalez A. 2017. Advances in the Myb–bHLH–Wd repeat (MBW) pigment regulatory model: Addition of a Wrky factor and Co-option of an anthocyanin Myb for betalain regulation. *Plant & Cell Physiology* **58(9)**:1431–1441. DOI: 10.1093/pcp/pcx075

Long W, Zou X, Zhang X. 2015. Transcriptome analysis of canola (*Brassica napus*) under salt stress at the germination stage. *PLOS ONE* **10(2)**:e0116217. DOI 10.1371/journal.pone.0116217

Luo H, Huo P, Wang Z, Zhang S, He Z, Wu Y, Zhao L, Liu J, Guo J, Fang S, Cao W, Yi L, Zhao Y, Kong L. 2021. KOBAS-i: Intelligent prioritization and exploratory visualization of biological functions for gene enrichment analysis. *Nucleic Acids Research* **49(W1)**:W317–W325. DOI 10.1093/nar/gkab447

Merico D, Isserlin R, Stueker O, Emili A, Bader GD. 2010. Enrichment map: A network-based method for gene-set enrichment visualization and interpretation. *PLOS ONE* **5(11)**:e13984 DOI 10.1371/journal.pone.0013984

Møller IS, Tester M. 2007. Salinity tolerance of *Arabidopsis*: A good model for cereals? *Trends in Plant Science* **12(12)**:534–540 DOI 10.1016/j.tplants.2007.09.009.

Møller IS, Gilliham M, Jha D, Mayo GM, Roy SJ, Coates JC, Haseloff J, Tester M. 2009. Shoot Na+ exclusion and increased salinity tolerance engineered by cell type-specific alteration of Na+ transport in *Arabidopsis*. *Plant Cell* **21(7)**:2163–2178 DOI 10.1105/tpc.108.064568.

Munns R, James RA, Xu B, Athman A, Conn SJ., Jordans C, Byrt CS, Hare RA, Tyerman SD, Tester M, Plett D, Gilliham M. 2012. Wheat grain yield on saline soils is improved by an ancestral Na^+ transporter gene. *Nature Biotechnology* **30**:360–364 DOI 10.1038/nbt.2120.

Munns R, Tester M. 2008. Mechanisms of salinity tolerance. *Annual Review of Plant Biology* **59**:651–681 DOI 10.1146/annurev.arplant.59.032607.092911.

Nguyen NH, Cheong JJ. 2018. H2A.Z-containing nucleosomes are evicted to activate AtMYB44 transcription in response to salt stress. *Biochemical Biophysical Research Communications* **499(4)**:1039–1043 DOI 10.1016/j.bbrc.2018.04.048.

Nakano T, Suzuki K, Fujimura T, Shinshi H. 2006. Genome-wide analysis of the ERF gene family in Arabidopsis and rice. *Plant Physiology* **140(2)**:411-432 DOI: 10.1104/pp.105.073783.

Nieves-Cordones M, Al Shiblawi FR, Sentenac H. 2016. Roles and transport of sodium and potassium in plants. *Metal Ions in Life Sciences* **16**:291-324 DOI 10.1007/978-3-319-21756-7_9.

Omrani S, Arzani A, Esmaeilzadeh Moghaddam ME, Mahlooji M. 2022. Genetic analysis of salinity tolerance in wheat (Triticum aestivum L.). *PLOS ONE* **17(3)**:e0265520 DOI 10.1371/journal.pone.0265520.

Oliveira DM, Mota TR, Salatta FV, Sinzker RC, Končitíková R, Kopečný D, Dos Santos WD. 2020. Cell wall remodeling under salt stress: Insights into changes in polysaccharides, feruloylation, lignification, and phenolic metabolism in maize. *Plant Cell & Environment* **43(9)**: 2172-2191 DOI: 10.1111/pce.13805

Peng Z, He S, Gong W, Sun J, Pan Z, Xu F, Lu Y, Du X. 2014. Comprehensive analysis of differentially expressed genes and transcriptional regulation induced by salt stress in two contrasting cotton genotypes. *BMC Genomics* **15**:1–28 DOI 10.1186/1471-2164-15-760.

Raudvere U, Kolberg L, Kuzmin I, Arak T, Adler P, Peterson H, Vilo JG. 2019. g:Profiler: A web server for functional enrichment analysis and conversions of gene lists (2019 update). *Nucleic Acids Research* **47(W1)**:W191–W198 DOI: 10.1093/nar/gkz369.

Riedelsberger J, Miller JK, Valdebenito-Maturana B, Piñeros MA, González W, Dreyer I. 2021. Plant HKT channels: An updated view on structure, function and gene regulation. *International Journal of Molecular Sciences* **22(4)**:1892 DOI 10.3390/ijms22041892.

Robinson MD, McCarthy DJ, Smyth GK. 2010. Edger: A bioconductor package for differential expression analysis of digital gene expression data. *Bioinformatics* **26(1)**:139–140 DOI 10.1093/bioinformatics/btp616.

Saade S, Brien C, Pailles Y, Berger B, Shahid M, Russell J, Waugh R, Negrão S, Tester M. 2020. Dissecting new genetic components of salinity tolerance in two-row spring barley at the vegetative and reproductive stages. *PLOS ONE* **15(7)**:e0236037 DOI 10.1371/journal.pone.0236037.

Sadak M S. 2019. Physiological role of trehalose on enhancing salinity tolerance of wheat plant. *Bulletin of National Research Centre* **43**:1–10 DOI: 10.1186/s42269-019-0098-6.

Sah SK, Reddy KR, Li J. 2016. Abscisic acid and abiotic stress tolerance in crop plants. *Frontiers in Plant Science* **7**:571 DOI 10.3389/fpls.2016.00571.

Sayed HI. 1985. Diversity of salt tolerance in a germplasm collection of wheat (*Triticum* spp.). *Theoretical and Applied Genetics* **69**:651–657 DOI 10.1007/BF00251118.

Schachtman DP, Schroeder JI. 1994. Structure and transport mechanism of a high-affinity potassium uptake transporter from higher plants. *Nature* **370(6491)**:655–658 DOI 10.1038/370655a0.

Seleiman M, Talha Aslam M, Ahmed Alhammad B, Umair Hassan M, Maqbool R, Umer Chattha M, Khan I, Ireri Gitari H, S Uslu O, Roy R, Leonardo Battaglia M. 2022. Salinity Stress in Wheat: Effects, Mechanisms and Management Strategies. *Phyton-International Journal of Experimental Botany* **91(4)**:667–694 DOI: 10.32604/phyton.2022.017365.

Seo JS, Sohn HB, Noh K, Jung C, An JH, Donovan CM, Somers DA. Kim DI, Jeong SC, Kim CG, Kim HM, Lee S, Choi YD, Moon TW, Kim CH, Cheong J. 2012. Expression of the Arabidopsis Atmyb44 gene confers drought/salt-stress tolerance in transgenic soybean. *Molecular Breeding* **29**:601–608 DOI 10.1007/s11032-011-9576-8.

Shavrukov Y, Langridge P, Tester M. 2009. Salinity tolerance and sodium exclusion in genus *Triticum*. *Breeding Science* **59(5)**:671–678. DOI 10.1270/jsbbs.59.671.

Shiferaw B, Smale M, Braun HJ, Duveiller E, Reynolds M, Muricho G. 2013. Crops that feed the world 10. Past successes and future challenges to the role played by wheat in global food security. *Food Security* **5**:291–317 DOI 10.1007/s12571-013-0263-y.

Singh V, Singh A., Bhadoria J, Giri J, Singh J, TV V, Sharma, PC. 2018. Differential expression of salt-responsive genes to salinity stress in salt-tolerant and salt-sensitive rice (*Oryza sativa* L.) at seedling stage. *Protoplasma* **255**:1667-1681 DOI 10.1007/s00709-018-1257-6

Singh DP, Sarkar RK. 2014. Distinction and characterisation of salinity tolerant and sensitive rice cultivars as probed by the chlorophyll fluorescence characteristics and growth parameters. *Functional Plant Biology* **41(7)**:727–736 DOI 10.1071/FP13229.

Sreenivasulu N, Usadel B, Winter A, Radchuk V, Scholz U, Stein N, Weschke W, Strickert M, Close TJ, Stitt M, Graner A, Wobus U. 2008. Barley grain maturation and germination: Metabolic pathway and regulatory network commonalities and differences highlighted by new MapMan/PageMan profiling tools. *Plant Physiology* **146(4)**:1738–1758 DOI 10.1104/pp.107.111781.

Subramanian A, Tamayo P, Mootha VK, Mukherjee S, Ebert BL, Gillette MA, Paulovich A, Pomeroy SL, Golub TR, Lander ES, Mesirov JP. 2005. Gene set enrichment analysis: A knowledge-based approach for interpreting genome-wide expression profiles. *Proceedings of the National Academy of Sciences* **102(43)**:15545–15550 DOI 10.1073/pnas.0506580102.

Tester M, Davenport R. 2003. Na^+ tolerance and Na^+ transport in higher plants. *Annals of Botany* **91(5)**:503–527 DOI 10.1093/aob/mcg058.

Tian F, Yang DC, Meng YQ, Jin J, Gao G. 2020. Plantregmap: Charting functional regulatory maps in plants. *Nucleic Acids Research* **48(D1)**:D1104–D1113 DOI 10.1093/nar/gkz1020.

Tohge T, de Souza LP, Fernie AR. 2017. Current understanding of the pathways of flavonoid biosynthesis in model and crop plants. *Journal of Experimental Botany* **68(15)**:4013–4028 DOI 10.1093/jxb/erx177.

Trujillo LE, Sotolongo M, Menéndez C, Ochogavía ME, Coll Y, Hernández I, Borrás-Hidalgo O, Thomma BP, Vera P, Hernández L. 2008. Soderf3, a novel sugarcane ethylene responsive factor (erf), enhances salt and drought tolerance when overexpressed in tobacco plants. *Plant & Cell Physiology* **49(4)**:512–525 DOI 10.1093/pcp/pcn025.

Tsai YC, Chen KC, Cheng TS, Lee C, Lin SH, Tung CW. 2019. Chlorophyll fluorescence analysis in diverse rice varieties reveals the positive correlation between the seedlings salt tolerance and photosynthetic efficiency. *BMC Plant Biology* **19**:1–517 DOI 10.1186/s12870-019-1983-8.

Vera Alvarez R, Pongor LS, Mariño-Ramírez L, Landsman D. 2019. TPMCalculator: One-step software to quantify mRNA abundance of genomic features. *Bioinformatics* **35(11)**:1960–1962 DOI 10.1093/bioinformatics/bty896.

Wu J, Yu C, Hunag L, Wu M, Liu B, Liu Y, Song G, Liu D, Gan Y. 2020. Overexpression of MADS-box transcription factor OsMADS25 enhances salt stress tolerance in Rice and Arabidopsis. *Plant Growth Regulation* **90**:163–171 DOI 10.1007/s10725-019-00539-6.

Xiong L, Yang Y. 2003. Disease resistance and abiotic stress tolerance in rice are inversely modulated by an abscisic acid-inducible mitogen-activated protein kinase. *Plant Cell* **15(3)**:745-759 DOI 10.1105/tpc.008714

Yang Q, Chen ZZ, Zhou X F, Yin HB, Li X, Xin XF, Hong XH, Zhu JK, Gong Z. 2009. Overexpression of SOS (salt overly sensitive) genes increases salt tolerance in transgenic Arabidopsis. *Molecular Plant* **2(1)**:22–31 DOI 10.1093/mp/ssn058.

Yang YY, Zheng PF, Ren YR, Yao YX, You CX, Wang XF, Hao YJ. 2021. Apple Mdsat1 encodes a bHLHm1 transcription factor involved in salinity and drought responses. *Planta* **253**:46 1–13 DOI 10.1007/s00425-020-03528-6.

Yuan YW, Sagawa JM, Frost L, Vela JP, Bradshaw HD Jr. 2014. Transcriptional control of floral anthocyanin pigmentation in monkeyflowers (*Mimulus*). *New Phytologist* **204(4)**:1013–1027 DOI 10.1111/nph.12968.

Zhang, S., Chen, C., Li, L., Meng, L., Singh, J., Jiang, N., & Lemaux, P. G. 2005. Evolutionary expansion, gene structure, and expression of the rice wall-associated kinase gene family. *Plant Physiology* **139(3)**:1107-1124 DOI 10.1104/pp.105.069005.

Zhang Y, Fang J, Wu X. Na Dong L 2018. Na+/K+ balance and transport Regulatory mechanisms in weedy and cultivated rice (*Oryza sativa* L.) under salt stress. *BMC Plant Biology* **18**:1–14 DOI 10.1186/s12870-018-1586-9.

Zhao PX, Zhang J, Chen SY, Wu J, Xia JQ, Sun LQ, Ma SS, Xiang CB. 2021. Arabidopsis MADS-box factor AGL16 is a negative regulator of plant response to salt stress by downregulating salt-responsive genes. *New Phytologist* **232(6)**:2418–2439 DOI 10.1111/nph.17760.

Zheng J, Wu H, Zhu H, Huang C, Liu C, Chang Y, Kong Z, Zhou Z, Wang G, Lin Y, Chen H. 2019. Determining factors, regulation system, and domestication of anthocyanin biosynthesis in rice leaves. *New Phytologist* **223(2)**:705–721 DOI 10.1111/nph.15807.

Zolman BK, Bartel B. 2004. An Arabidopsis indole-3-butyric acid-response mutant defective in PEROXIN6, an apparent ATPase implicated in peroxisomal function. *Proceedings of the National Academy of Sciences* **101(6)**:1786–1791 DOI 10.1073/pnas.0304368101.

Figure titles and legends

Figure 1. Effect of salt stress on seed germination and seedling growth.
(A) Germination rate of wheat seeds under different salt concentrations. 500 seeds from each line were placed on two layers of germination paper and exposed to a solution containing 150mM NaCl in a phytohealth chamber (SPL Life Sciences) at a temperature of 22°C. Germination was assessed after 4 days. (B) Wheat seedling growth under different salinity levels. Seven-day-old seedlings were subjected to a salt stress treatment with a total volume of 200ml of the solution containing 150mM NaCl after 4 days. (C) Phenotypes of wheat seedlings under different salinity levels after 4 days of salt stress with a total volume of 200ml of the solution containing 150mM NaCl. (D) Shoot and root lengths of wheat seedlings under different salinity conditions after 4 days of salt stress with a total volume of 200ml of the solution containing 150mM NaCl. Independent t-tests demonstrated significant differences (* $p < 0.05$ and ** $p < 0.01$).

Figure 2. Na^+ and K^+ ion contents, differential ratios of K^+ and Na^+ and chlorophyll concentrations for PL1 and PL6 under salt stress treatment.
Seven-day-old seedlings were subjected to a salt stress treatment with a total volume of 200ml of the solution containing 150mM NaCl. After treatment with 150 mM NaCl, wheat leaves were collected at 0, 3, 24, and 48 hours. (A) Na+ ion content in the shoots under different salt stress exposure times. (B) K+ ion content in the shoots under different salt stress exposure times. (C) Changes in the relative "Na+ ratio" in shoots at different time points after salt stress treatment. The "Na+ ratio" represents the relative proportion of Na+ content in shoots compared to the Na+ content at 0 hours (baseline). Data points at 3 hours, 24 hours, and 48 hours indicate the fold change of Na+ content in shoots compared to the baseline (0 hours). (D) Changes in the relative "K+ ratio" in shoots at different time points after salt stress treatment. The "K+ ratio" represents the relative proportion of K+ content in shoots compared to the K+ content at 0 hours (baseline). Data points at 3 hours, 24 hours, and 48 hours indicate the fold change of K+ content in shoots compared to the baseline (0 hours). (E) Chlorophyll concentrations in the shoots under different salt stress exposure times. Each bar represents the mean ± standard error (n = 3). Independent t-tests showed significant differences (* $p < 0.05$ and ** $p < 0.01$).

Figure 3. Differentially expressed genes (DEGs) and Gene Set Enrichment Analysis (GSEA) for PL1 and PL6.
(A) Venn diagrams showing the number of DEGs between PL1 and PL6 and the overlap of all DEGs at different time points after exposure to salt stress. (B) Number of DEGs only expressed in PL1 at different time points after exposure to salt stress. (C) Number of DEGs only expressed in PL6 at different time points after exposure to salt stress. (D) GSEA enrichment analysis with gene ontology of the DEGs. Dots indicate significant GO terms from the pairwise gene set enrichment analysis comparisons at each time point after exposure to salt stress. The size of the dots indicates the number of genes, and the color of the dots indicates the −log10 FDR value within the pathway.

Figure 4. Gene ontology (GO) Enrichment Map and differential gene expression profiling for PL1 and PL6.
(A–E) Five networks of significantly enriched gene sets between PL1 and PL6 obtained on the Enrichment Map. Nodes representing enriched gene sets were classified based on their similarity to related gene sets. The size of the node is proportional to the total number of genes. The thickness of the green line between nodes represents the proportion of shared genes between gene sets. (F–

J) The expression patterns of each network at each time point after exposure to salt stress. Each cluster represents a group of functionally related gene sets that showed similar expression patterns. Figure 4F, 4G, 4H, 4I, and 4J show multiple clusters derived from the networks of Figures 4A, 4B, 4C, 4D, and 4E, respectively. Clusters showing different expression patterns between PL1 and PL6 were indicated in red boxes. (K) Heatmaps representing the expressions of differentially expressed genes (DEGs) marked in red boxes (F, G, and I) for PL1 and PL6.

Figure 5. Gene Set Enrichment Analysis with Kyoto Encyclopedia of Genes and Genomes (KEGG) pathways of the differentially expressed genes (DEGs).
Dots represent significant KEGG pathways from the pairwise gene set enrichment analysis comparisons at each time point after exposure to salt stress. The size of the dots indicates the number of differential genes, while the color of the dots represents the p-values of enrichment analysis. The rich factor refers to the ratio of the number of DEGs in the pathway to the total number of genes. The size of the dots indicates the number of genes, and the color of the dots indicates the −log10 FDR value within the pathway.

Figure 6. Differentially expressed transcription factors (TFs) under salt stress treatment in PL1 and PL6.
(A) Distribution of TF family members among the differentially expressed genes (DEGs). The bar graph illustrates the number of TFs belonging to each TF family among the DEGs. (B) Expression patterns of TFs at each time point after exposure to salt stress. Each cluster with similar expression patterns is indicated by red boxes. (C) Heatmap analysis of TF family genes in PL1 and PL6 under salt stress treatment, with the genes marked by red boxes in (B) specifically highlighted.

Figure 7. Biochemical assays of antioxidant enzyme activity.
(A) Catalase (CAT) activity, (B) Peroxidase (POD) activity, (C) Total Superoxide Dismutase (SOD) activity, and (D) Total Antioxidant Capacity (TAC). Each bar represents the average ± standard error (n = 3). Independent t-tests demonstrated significant differences (* $p < 0.05$ and ** $p < 0.01$) compared to the control condition (0h).

Figure 8. Validation of the RNA sequencing results via reverse transcription-quantitative polymerase chain reaction (RT-qPCR) at different timepoints under salt stress conditions.
Three clusters representing different expression patterns for PL1 and PL6 were selected and the relative expressions shown. RT-qPCR was performed with three biological replicates. Each bar represents the average ± standard error ($n = 3$). Independent t-tests showed significant differences (* $p < 0.05$ and ** $p < 0.01$)

Supplemental information Titles and Legends

Supplementary Figure 1 (Fig. S1). Field images of M6 generations of PL1 and PL6 at different time points.
(A) Plot images of M6 generations of PL1 and PL6 at different time points. (B) and (C) Different views of the field at various time points. The dates when the photos were taken are indicated below each image.

Supplementary Figure 2 (Fig. S2). Comparison of seed coat color of different wheat lines.

PL1 (control) and PL6 (mutant lines) were used in this study. Additionally, Chengwoo and Keumkang are two of the cultivars commonly grown in South Korea.

Supplementary Figure 3 (Fig. S3). Comparison of salt stress response in mutant lines (PL2-PL49) and wild type control (PL1).

(A) Germination rate of mutant lines (PL2-PL49) and PL1 as the wild type control. (B) Shoot length of mutant lines (PL2-PL49) and PL1 as the wild type control. (C) Root length of mutant lines (PL2-PL49) and PL1 as the wild type control. For the preliminary screening of the selected mutant lines, 100 seeds from each line were placed in a phytohealth chamber (SPL Life Sciences) with two layers of germination paper, and a total volume of 200ml of the solution containing 150mM NaCl was applied to them at a temperature of 22°C. After 4 days, the germination rate, shoot length, and root length were recorded. PL1 served as the wild type control in these experiments.

Supplementary Table 1 (Table S1). The details of the primers used in this study.

Supplementary Table 2 (Table S2). Germination ratio the different salt concentrations on seed germination.

Supplementary Table 3 (Table S3). Summary of RNA-seq quality, read counts, and mapping rates.

Supplementary Table 4 (Table S4). Differentially expressed genes (DEGs) from BlastX results against NCBI Poaceae family.

This table contains the blastx results against the NCBI *Poaceae* family, which led to the identification of a total of 4,017 differentially expressed genes (DEGs) with a p-value < 0.05 and FDR < 0.05.

Supplementary Table 5 (Table S5). Gene Set Enrichment Analysis (GSEA) for PL1 and PL6 using gene ontology (GO) mapping of differentially expressed genes.

Supplementary Table 6 (Table S6). Gene Set Enrichment Analysis (GSEA) for PL1 and PL6 using Kyoto Encyclopedia of Genes and Genomes (KEGG) pathways mapping of differentially expressed genes.

Supplementary Table 7 (Table S7). Differentially express genes in red boxes of Fig. 6B used in Fig. 6C.

Figure 1

Figure 1. Effect of salt stress on seed germination and seedling growth.

(A) Germination rate of wheat seeds under different salt concentrations. 500 seeds from each line were placed on two layers of germination paper and exposed to a solution containing 150mM NaCl in a phytohealth chamber (SPL Life Sciences) at a temperature of 22°C. Germination was assessed after 4 days. (B) Wheat seedling growth under different salinity levels. Seven-day-old seedlings were subjected to a salt stress treatment with a total volume of 200ml of the solution containing 150mM NaCl after 4 days. (C) Phenotypes of wheat seedlings under different salinity levels after 4 days of salt stress with a total volume of 200ml of the solution containing 150mM NaCl. (D) Shoot and root lengths of wheat seedlings under different salinity conditions after 4 days of salt stress with a total volume of 200ml of the solution containing 150mM NaCl. Independent t-tests demonstrated significant differences (* $p < 0.05$ and ** $p < 0.01$).

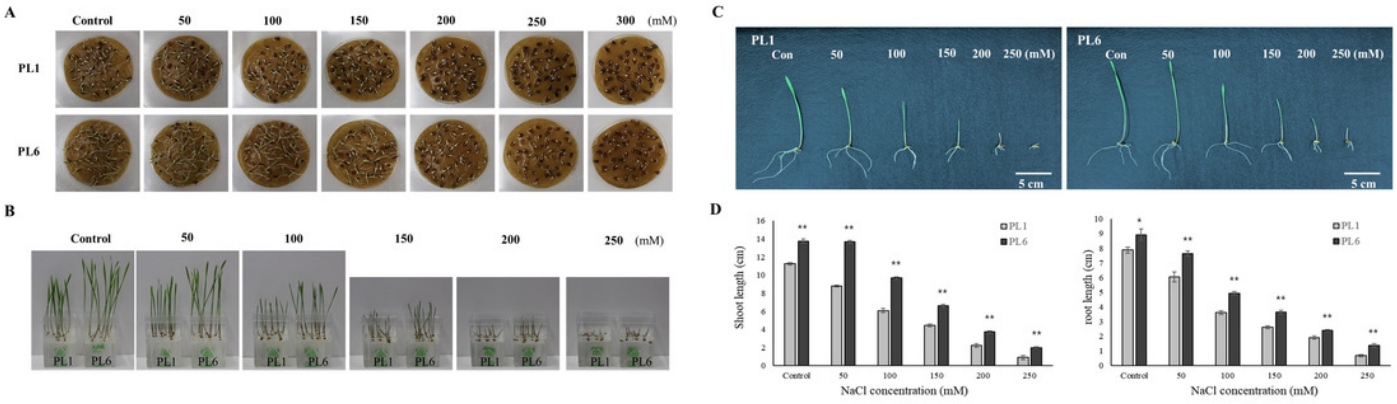
A
Control
50
100
150
200
250
300 (mM)
PL1
PL6
B
Control
50
100
150
200
250 (mM)
PL1 PL6
C
PL1
Con
50
100
150
200
250 (mM)
5 cm
PL6
Con
50
100
150
200
250 (mM)
5 cm
D
PL1
PL6
Shoot length (cm)
NaCl concentration (mM)
root length (cm)
NaCl concentration (mM)

Figure 2

Figure 2. Na^+ and K^+ ion contents, differential ratios of K^+ and Na^+ and chlorophyll concentrations for PL1 and PL6 under salt stress treatment.

Seven-day-old seedlings were subjected to a salt stress treatment with a total volume of 200ml of the solution containing 150mM NaCl. After treatment with 150 mM NaCl, wheat leaves were collected at 3, 24, and 48 hours. (A) Na^+ ion content in the shoots under different salt stress exposure times. (B) K^+ ion content in the shoots under different salt stress exposure times. (C) Changes in the relative "Na^+ ratio" in shoots at different time points after salt stress treatment. The "Na^+ ratio" represents the relative proportion of Na^+ content in shoots compared to the Na^+ content at 0 hours (baseline). Data points at 3 hours, 24 hours, and 48 hours indicate the fold change of Na+ content in shoots compared to the baseline (0 hours). (D) Changes in the relative "K^+ ratio" in shoots at different time points after salt stress treatment. The "K^+ ratio" represents the relative proportion of K^+ content in shoots compared to the K^+ content at 0 hours (baseline). Data points at 3 hours, 24 hours, and 48 hours indicate the fold change of K^+ content in shoots compared to the baseline (0 hours). (E) Chlorophyll concentrations in the shoots under different salt stress exposure times. Each bar represents the mean ± standard error (n = 3). Independent t-tests showed significant differences (* $p < 0.05$ and ** $p < 0.01$).

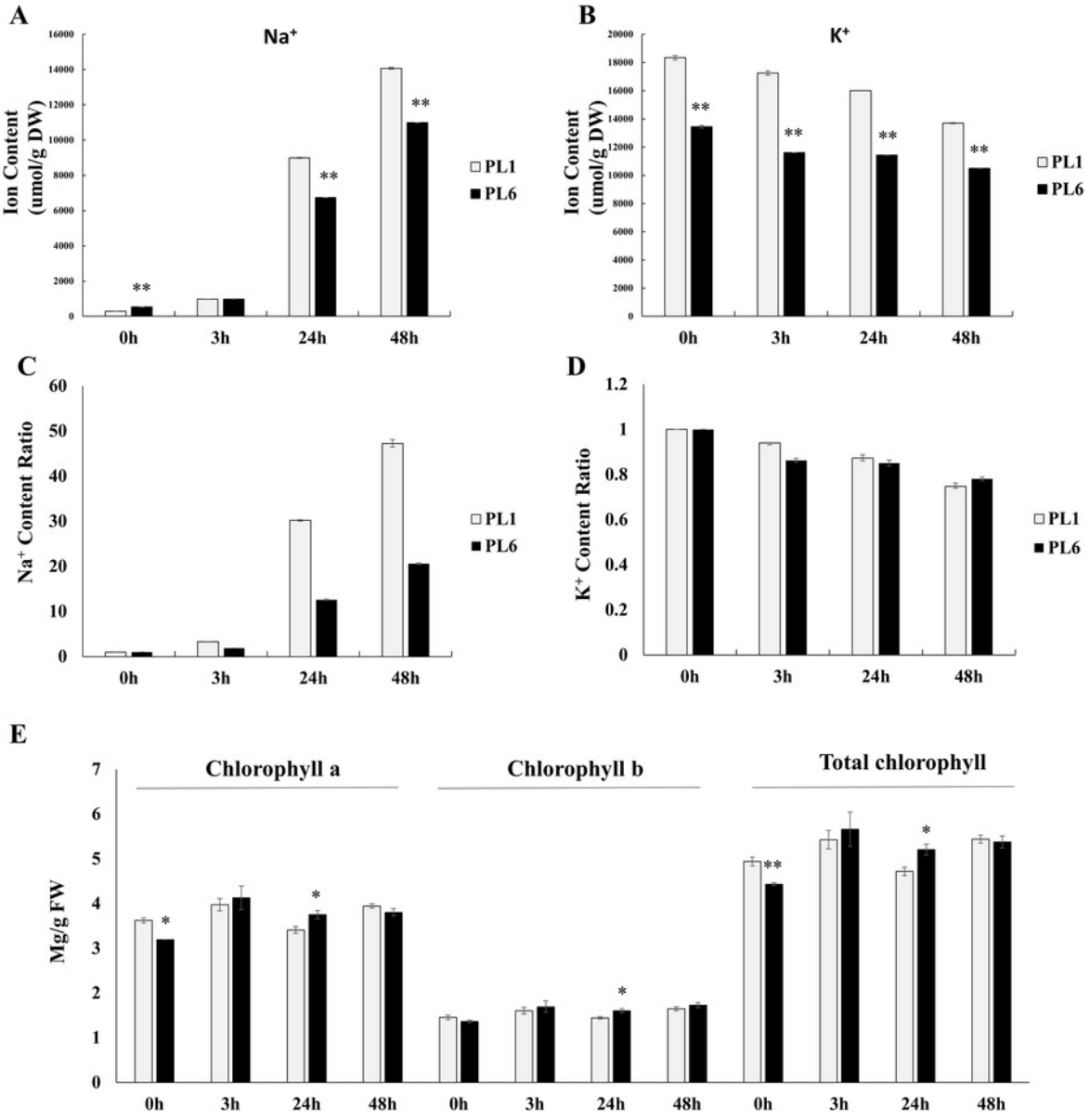
A
Na+
Ion Content (umol/g DW)
PL1
PL6
0h
3h
24h
48h
B
K+
Ion Content (umol/g DW)
C
Na+ Content Ratio
D
K+ Content Ratio
E
Chlorophyll a
Chlorophyll b
Total chlorophyll
Mg/g FW

Figure 3

Figure 3. Differentially expressed genes (DEGs) and Gene Set Enrichment Analysis (GSEA) for PL1 and PL6.

(A) Venn diagrams showing the number of DEGs between PL1 and PL6 and the overlap of all DEGs at different time points after exposure to salt stress. (B) Number of DEGs only expressed in PL1 at different time points after exposure to salt stress. (C) Number of DEGs only expressed in PL6 at different time points after exposure to salt stress. (D) GSEA enrichment analysis with gene ontology of the DEGs. Dots indicate significant GO terms from the pairwise gene set enrichment analysis comparisons at each time point after exposure to salt stress. The size of the dots indicates the number of genes, and the color of the dots indicates the −log10 FDR value within the pathway.

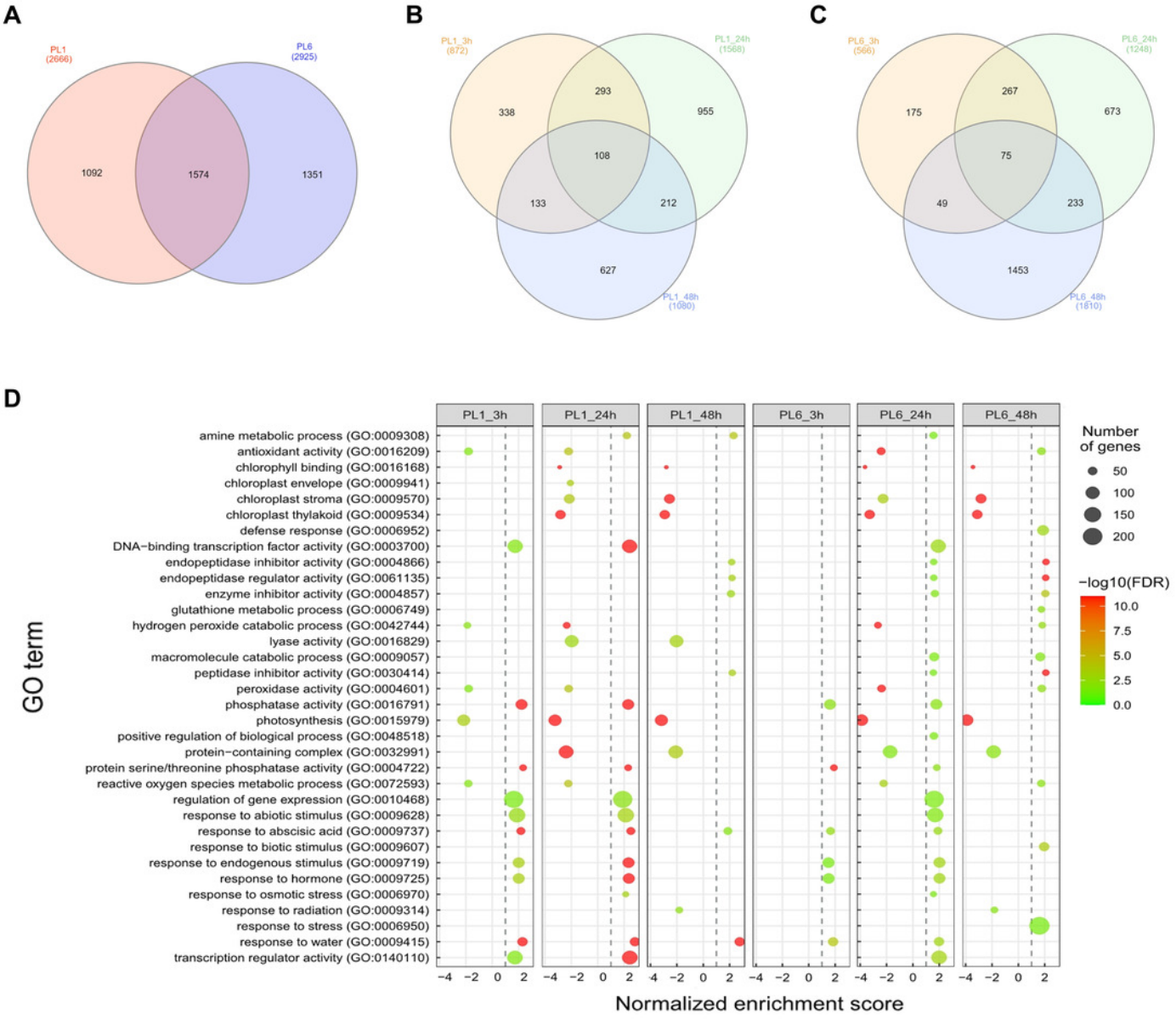
A
PL1
(2666)
PL6
(2925)
1092
1574
1351
B
PL1_3h
(872)
PL1_24h
(1568)
PL1_48h
(1080)
338
293
955
108
133
212
627
C
PL6_3h
(566)
PL6_24h
(1248)
PL6_48h
(1610)
175
267
673
75
49
233
1453
D
PL1_3h
PL1_24h
PL1_48h
PL6_3h
PL6_24h
PL6_48h
GO term
amine metabolic process (GO:0009308)
antioxidant activity (GO:0016209)
chlorophyll binding (GO:0016168)
chloroplast envelope (GO:0009941)
chloroplast stroma (GO:0009570)
chloroplast thylakoid (GO:0009534)
defense response (GO:0006952)
DNA−binding transcription factor activity (GO:0003700)
endopeptidase inhibitor activity (GO:0004866)
endopeptidase regulator activity (GO:0061135)
enzyme inhibitor activity (GO:0004857)
glutathione metabolic process (GO:0006749)
hydrogen peroxide catabolic process (GO:0042744)
lyase activity (GO:0016829)
macromolecule catabolic process (GO:0009057)
peptidase inhibitor activity (GO:0030414)
peroxidase activity (GO:0004601)
phosphatase activity (GO:0016791)
photosynthesis (GO:0015979)
positive regulation of biological process (GO:0048518)
protein−containing complex (GO:0032991)
protein serine/threonine phosphatase activity (GO:0004722)
reactive oxygen species metabolic process (GO:0072593)
regulation of gene expression (GO:0010468)
response to abiotic stimulus (GO:0009628)
response to abscisic acid (GO:0009737)
response to biotic stimulus (GO:0009607)
response to endogenous stimulus (GO:0009719)
response to hormone (GO:0009725)
response to osmotic stress (GO:0006970)
response to radiation (GO:0009314)
response to stress (GO:0006950)
response to water (GO:0009415)
transcription regulator activity (GO:0140110)
−4 −2 0 2
Normalized enrichment score
Number
of genes
50
100
150
200
−log10(FDR)
10.0
7.5
5.0
2.5
0.0

Figure 4

Figure 4. Gene ontology (GO) Enrichment Map and differential gene expression profiling for PL1 and PL6.

(A–E) Five networks of significantly enriched gene sets between PL1 and PL6 obtained on the Enrichment Map. Nodes representing enriched gene sets were classified based on their similarity to related gene sets. The size of the node is proportional to the total number of genes. The thickness of the green line between nodes represents the proportion of shared genes between gene sets. (F–J) The expression patterns of each network at each time point after exposure to salt stress. Each cluster represents a group of functionally related gene sets that showed similar expression patterns. Figure 4F, 4G, 4H, 4I, and 4J show multiple clusters derived from the networks of Figures 4A, 4B, 4C, 4D, and 4E, respectively. Clusters showing different expression patterns between PL1 and PL6 were indicated in red boxes. (K) Heatmaps representing the expressions of differentially expressed genes (DEGs) marked in red boxes (F, G, and I) for PL1 and PL6.

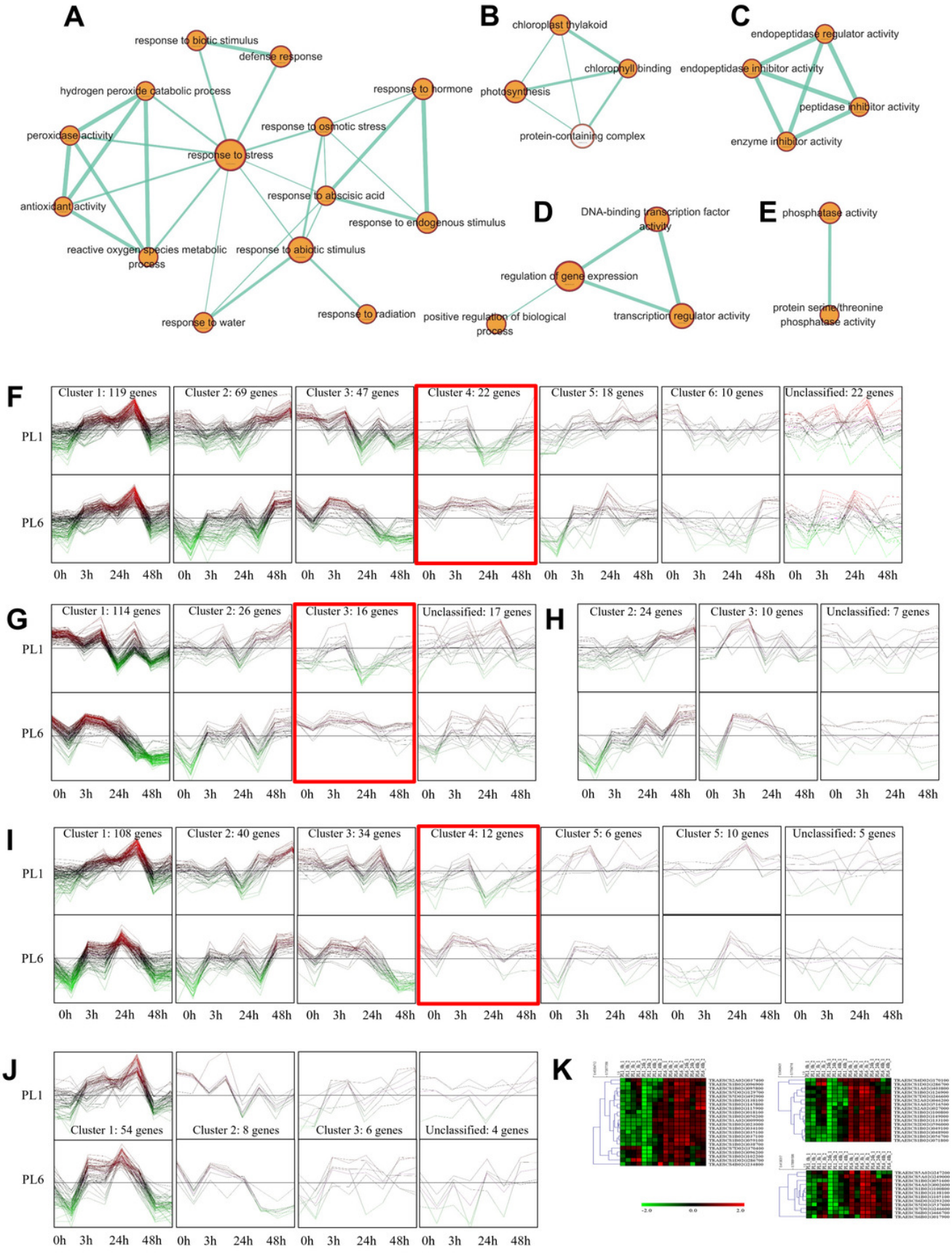
A
response to biotic stimulus
defense response
hydrogen peroxide catabolic process
response to hormone
response to osmotic stress
peroxidase activity
response to stress
antioxidant activity
response to abscisic acid
response to endogenous stimulus
reactive oxygen species metabolic process
response to abiotic stimulus
response to water
response to radiation
B
chloroplast thylakoid
chlorophyll binding
photosynthesis
protein-containing complex
C
endopeptidase regulator activity
endopeptidase inhibitor activity
peptidase inhibitor activity
enzyme inhibitor activity
D
DNA-binding transcription factor activity
regulation of gene expression
positive regulation of biological process
transcription regulator activity
E
phosphatase activity
protein serine/threonine phosphatase activity
F
Cluster 1: 119 genes
Cluster 2: 69 genes
Cluster 3: 47 genes
Cluster 4: 22 genes
Cluster 5: 18 genes
Cluster 6: 10 genes
Unclassified: 22 genes
PL1
PL6
0h 3h 24h 48h
G
Cluster 1: 114 genes
Cluster 2: 26 genes
Cluster 3: 16 genes
Unclassified: 17 genes
H
Cluster 2: 24 genes
Cluster 3: 10 genes
Unclassified: 7 genes
I
Cluster 1: 108 genes
Cluster 2: 40 genes
Cluster 3: 34 genes
Cluster 4: 12 genes
Cluster 5: 6 genes
Cluster 5: 10 genes
Unclassified: 5 genes
J
Cluster 1: 54 genes
Cluster 2: 8 genes
Cluster 3: 6 genes
Unclassified: 4 genes
K

Figure 5

Figure 5. Gene Set Enrichment Analysis with Kyoto Encyclopedia of Genes and Genomes (KEGG) pathways of the differentially expressed genes (DEGs).

Dots represent significant KEGG pathways from the pairwise gene set enrichment analysis comparisons at each time point after exposure to salt stress. The size of the dots indicates the number of differential genes, while the color of the dots represents the p-values of enrichment analysis. The rich factor refers to the ratio of the number of DEGs in the pathway to the total number of genes. The size of the dots indicates the number of genes, and the color of the dots indicates the −log10 FDR value within the pathway.

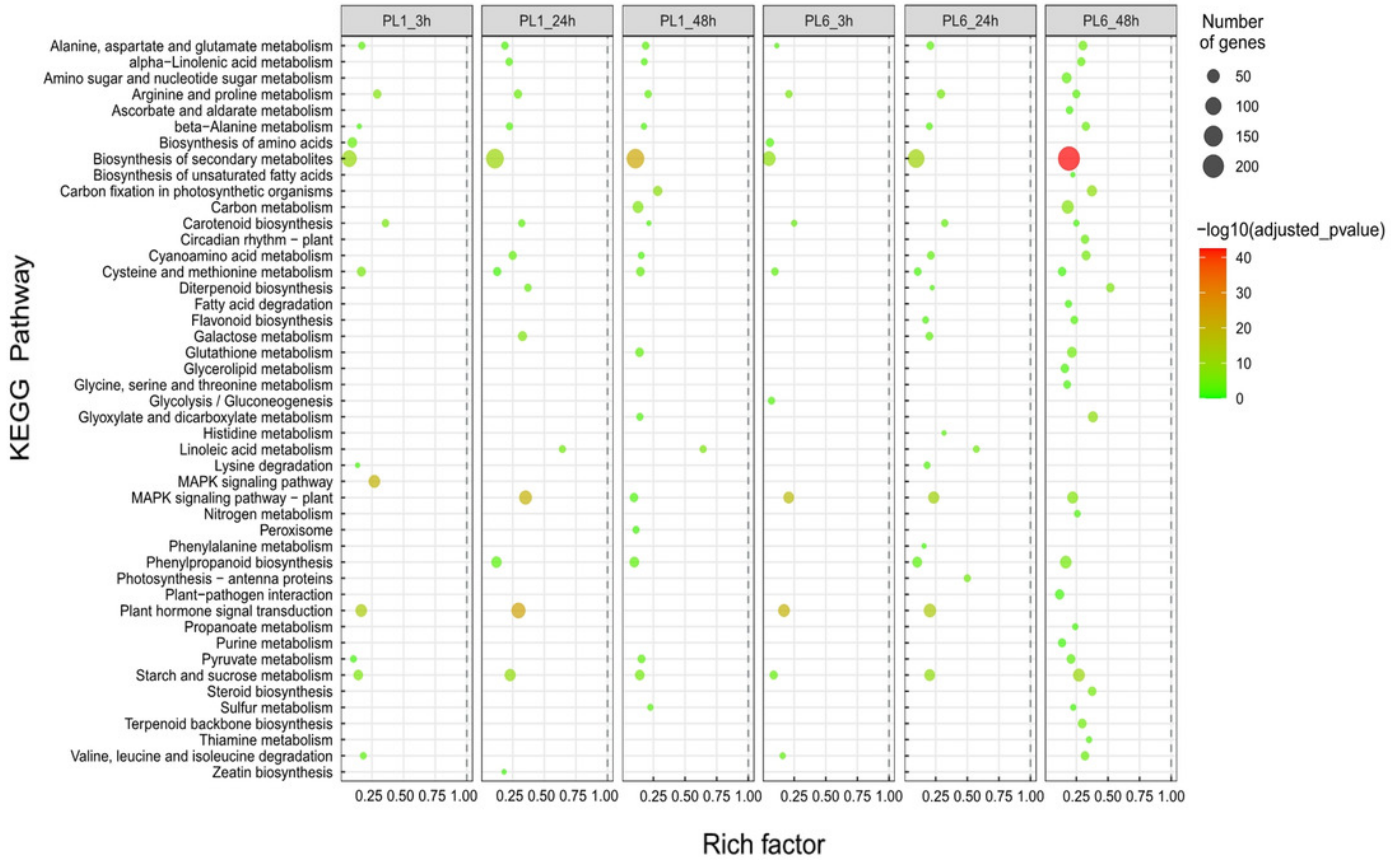

Figure 6

Figure 6. Differentially expressed transcription factors (TFs) under salt stress treatment in PL1 and PL6.

(A) Distribution of TF family members among the differentially expressed genes (DEGs). The bar graph illustrates the number of TFs belonging to each TF family among the DEGs. (B) Expression patterns of TFs at each time point after exposure to salt stress. Each cluster with similar expression patterns is indicated by red boxes. (C) Heatmap analysis of TF family genes in PL1 and PL6 under salt stress treatment, with the genes marked by red boxes in (B) specifically highlighted.

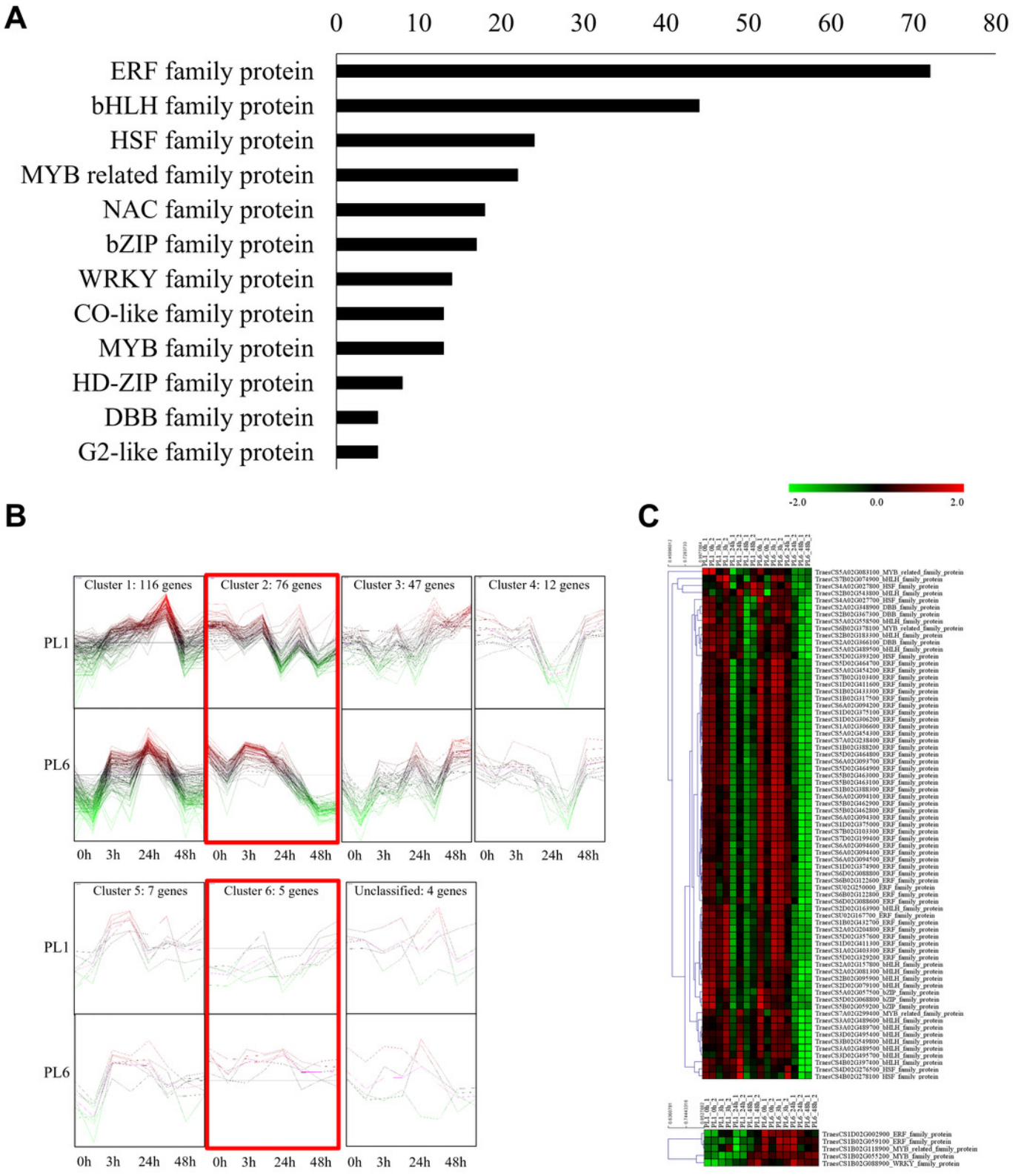
A
0
10
20
30
40
50
60
70
80
ERF family protein
bHLH family protein
HSF family protein
MYB related family protein
NAC family protein
bZIP family protein
WRKY family protein
CO-like family protein
MYB family protein
HD-ZIP family protein
DBB family protein
G2-like family protein
B
Cluster 1: 116 genes
Cluster 2: 76 genes
Cluster 3: 47 genes
Cluster 4: 12 genes
PL1
PL6
0h 3h 24h 48h 0h 3h 24h 48h 0h 3h 24h 48h 0h 3h 24h 48h
Cluster 5: 7 genes
Cluster 6: 5 genes
Unclassified: 4 genes
PL1
PL6
0h 3h 24h 48h 0h 3h 24h 48h 0h 3h 24h 48h
C
-2.0
0.0
2.0

Figure 7

Figure 7. Biochemical assays of antioxidant enzyme activity.

(A) Catalase (CAT) activity, (B) Peroxidase (POD) activity, (C) Total Superoxide Dismutase (SOD) activity, and (D) Total Antioxidant Capacity (TAC). Each bar represents the average ± standard error (n = 3). Independent t-tests demonstrated significant differences (* $p < 0.05$ and ** $p < 0.01$) compared to the control condition (0h).

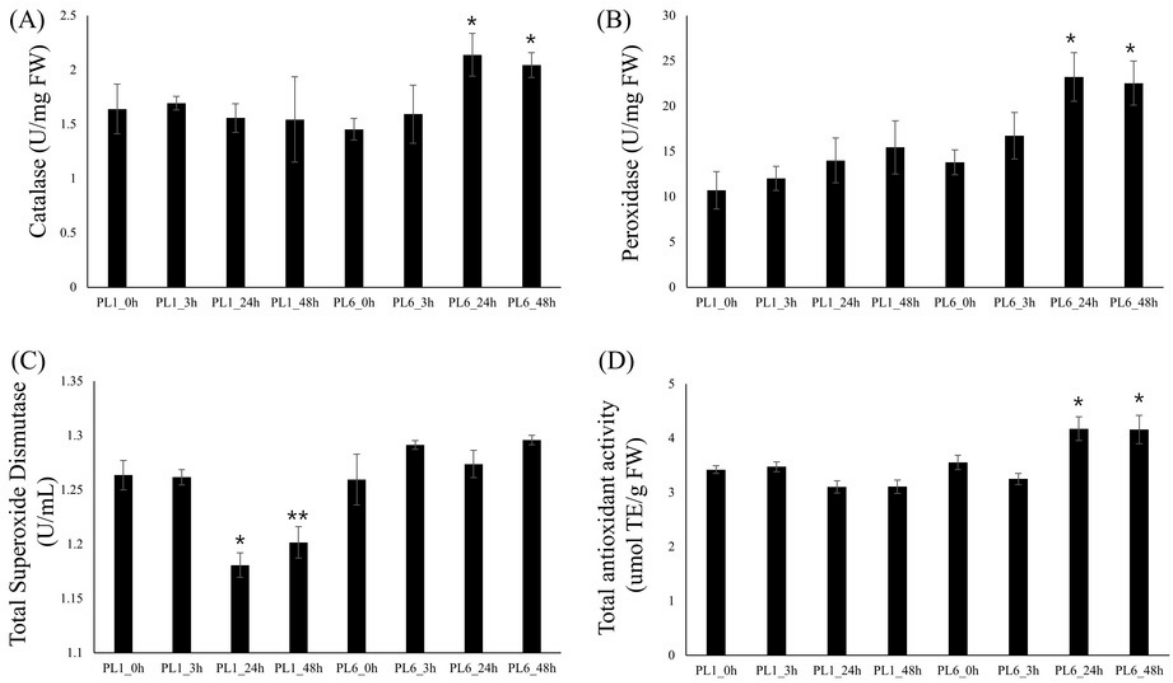

Figure 8

Figure 8. Validation of the RNA sequencing results via reverse transcription-quantitative polymerase chain reaction (RT-qPCR) at different timepoints under salt stress conditions.

Three clusters representing different expression patterns for PL1 and PL6 were selected and the relative expressions shown. RT-qPCR was performed with three biological replicates. Each bar represents the average ± standard error (n = 3). Independent t-tests showed significant differences (* $p < 0.05$ and ** $p < 0.01$)

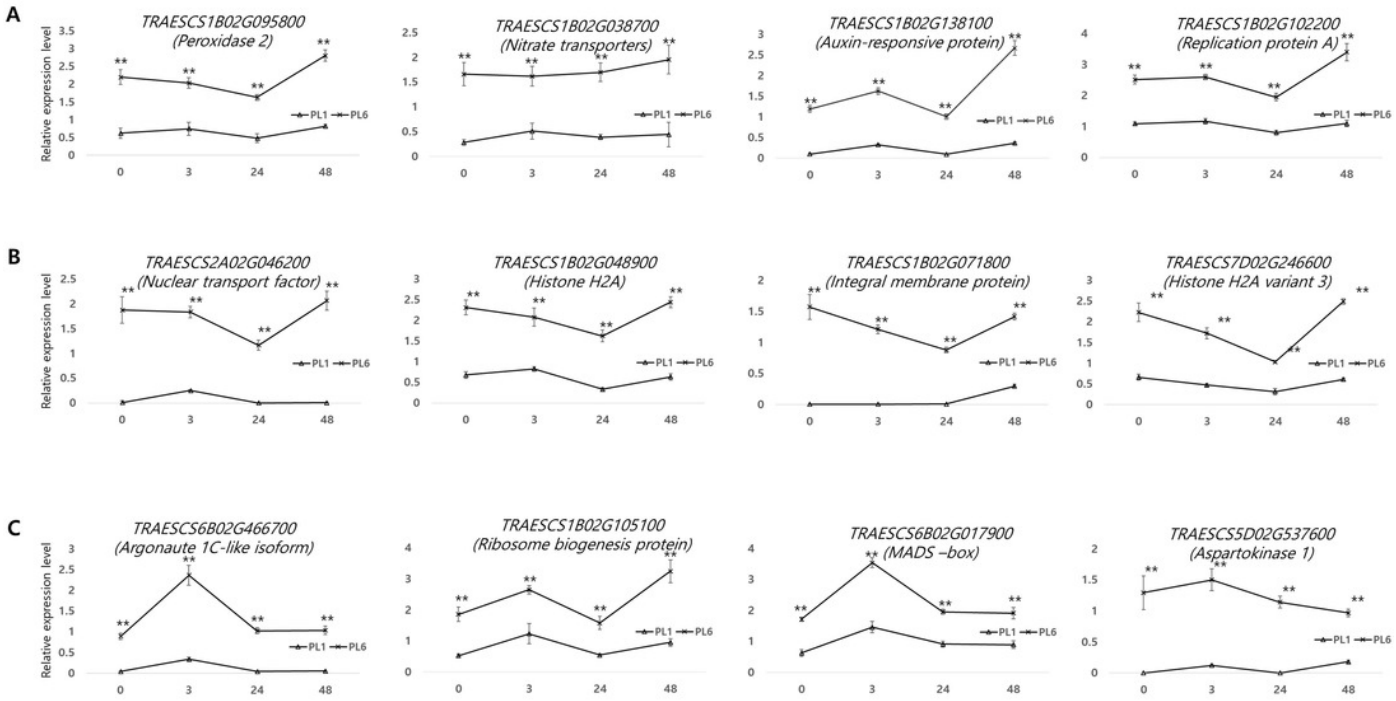

Table 1(on next page)

Table 1. List of differentially expressed genes selected by K-means clustering from GSEA analysis

Table 1:

List of differentially expressed genes selected by K-means clustering from GSEA analysis.

Gene ID	Description	Length	E-value	Similarity (%)	Log2 fold change (PL6/PL1)				p-value	FDR	Group
					0 h	3 h	12 h	24 h			
TRAESCS1B02G145800	abscisic acid receptor PYL8	205	1E-149	92.57	**4.37**	1.96	**7.28**	1.87	2.09E-19	2.53E-29	
TRAESCS1B02G138100	auxin-responsive protein IAA15	198	2E-143	81.71	**3.64**	1.88	**3.57**	**2.42**	1.56E-28	6.22E-36	
TRAESCS5D02G129700	chaperone protein dnaJ GFA2, mitochondrial	421	0	84.11	**8.75**	1.57	**6.56**	**5.69**	4.77E-38	7.45E-69	
TRAESCS1B02G018100	defensin	81	1.1E-38	84.72	**4.86**	**7.74**	**5.55**	−0.43	1.82E-09	4.81E-93	
TRAESCS1B02G059100	dehydroascorbate reductase	212	9E-156	95.77	**3.75**	**3.64**	**3.78**	1.76	4.05E-69	4.52E-24	DEGs in red boxes of cluster 4 in Fig. 4F
TRAESCS1B02G050200	E3 ubiquitin-protein ligase XB3	486	0	82.96	**3.96**	**3.92**	**4.48**	1.15	1.98E-36	9.28E-17	
TRAESCS5D02G492900	heat shock cognate 70 kDa protein 2	614	0	92.5	**3.67**	1.74	**3.52**	**3.68**	6.04E-97	2.97E-66	
TRAESCS1B02G037100	NAD(P)-binding Rossmann-fold superfamily protein	300	0	91.03	**5.36**	**4.72**	**5.49**	**2.27**	5.67E-67	1.12E-26	
TRAESCS1B02G095800	Peroxidase 2	340	0	89.71	**7.85**	1.71	**7.13**	**2.85**	8.69E-72	9.78E-22	
TRAESCS1B02G096200	peroxidase 5	338	0	85.36	**4.99**	1.58	**4.80**	1.88	1.81E-23	3.68E-64	
TRAESCS1B02G096900	Peroxidase 5	343	0	75.36	**4.34**	1.12	**3.82**	**3.15**	7.29E-26	8.91E-18	
TRAESCS1B02G115900	peroxidase A2-like	342	0	82.95	**3.84**	**2.45**	**4.16**	**3.27**	5.42E-59	3.96E-69	
TRAESCS1B02G038700	protein NRT1/ PTR FAMILY 6.2	582	0	90.52	**7.36**	**8.20**	**8.09**	1.46	1.78E-64	2.32E-34	
TRAESCS1A02G009900	putative disease resistance RPP13-like protein 3	844	0	82.63	**6.88**	**6.49**	**6.40**	−1.81	1.3E-14	2.22E-56	

TRAESCS1B02G023000	putative disease resistance RPP13-like protein 3	920	0	72.15	**7.98**	**8.61**	**7.67**	**2.83**	2.09E-29	9.97E-62	
TRAESCS1B02G102200	replication protein A 70 kDa DNA-binding subunit C-like	881	0	73.55	**4.59**	0.95	**7.35**	2.00	2.3E-18	1.6E-27	
TRAESCS2A02G037400	stress-response A/B barrel domain-containing protein HS1	115	9E-76	85.48	**8.11**	1.65	**8.58**	**8.10**	2.94E-31	2.53E-29	
TRAESCS1B02G034100	subtilisin-chymotrypsin inhibitor CI-1B	74	1.8E-44	84.47	**9.97**	**11.00**	**11.50**	**3.89**	4.45E-72	3.44E-77	
TRAESCS1B02G035100	subtilisin-chymotrypsin inhibitor CI-1B	74	2.3E-45	84.72	**10.70**	**11.55**	**12.07**	**2.56**	2.35E-80	4.03E-13	
TRAESCS4D02G170100	60S ribosomal protein L19-1	228	2E-144	88.22	**7.03**	−0.34	**7.73**	−7.05	5.65E-47	1.2E-44	
TRAESCS2A02G027000	actin-related protein 9 isoform X1	526	0	84.59	**5.48**	1.33	**3.59**	**2.19**	6.68E-81	1.05E-77	
TRAESCS1B02G133100	DNA-directed RNA polymerases II, IV and V subunit 11	119	2E-86	96.77	**8.01**	**2.08**	**8.31**	**2.82**	7.37E-23	3.82E-21	
TRAESCS2D02G596000	exocyst complex component EXO70A1	637	0	93.63	**6.65**	**2.49**	**5.61**	**2.78**	7.27E-83	1.44E-79	
TRAESCS1B02G048900	histone H2A	154	1E-99	92.72	**5.66**	**5.03**	**6.05**	**3.09**	2.91E-11	6.97E-10	
TRAESCS1B02G049100	histone H2A	155	1E-98	91.26	**7.65**	**8.17**	**8.49**	**3.42**	4.73E-34	4.76E-32	
TRAESCS1D02G286700	histone H4	103	6.6E-70	99.76	**3.41**	−1.75	**2.65**	0.70	6.57E-35	6.97E-33	
TRAESCS1B02G149000	INO80 complex subunit D	288	0	82.89	**7.67**	1.69	**7.82**	**2.84**	6.2E-18	3.82E-21	
TRAESCS1B02G126900	NAD(P)H-quinone oxidoreductase subunit S, chloroplastic	239	6E-167	82.95	**3.54**	1.97	**3.25**	1.86	3.85E-37	2.43E-16	
TRAESCS2A02G046200	nuclear transport factor 2 (NTF2)-	199	4E-	82.59	**8.80**	**2.01**	**8.64**	**8.71**	6.74E-30	6.97E-33	

DEGs in red boxes of cluster 3 in Fig. 4G

	like protein		115								
TRAESCS1A02G403800	predicted protein	266	0	96.99	**2.85**	**2.44**	**2.78**	1.30	0.006931	1.05E-77	
TRAESCS7D02G370400	predicted protein	312	0	83.35	**2.11**	-0.21	**3.22**	**2.03**	8.65E-36	5.3E-28	
TRAESCS7D02G246600	probable histone H2A variant 3	139	3E-95	95.7	**2.08**	1.78	**3.65**	**2.75**	1.62E-42	1.44E-79	
TRAESCS3A02G516500	Protein COFACTOR ASSEMBLY OF COMPLEX C SUBUNIT B CCB3, chloroplastic	192	4E-117	76.6	**7.91**	**2.26**	**8.02**	**8.40**	4.51E-69	3.25E-66	
TRAESCS 1B02G100800	RNA-binding protein 8A	209	9E-152	85.74	**4.77**	1.01	**4.64**	**2.08**	7.57E-28	1.2E-44	
TRAESCS 1B02G071800	thylakoid membrane protein TERC, chloroplastic	377	0	84.39	**9.49**	**8.95**	**9.08**	1.70	3.6E-18	2.67E-40	
TRAESCS 1B02G056700	translation initiation factor IF-2 isoform X1	239	7E-174	78.99	**6.41**	**8.58**	**5.77**	**2.58**	5.67E-56	9.72E-34	
TRAESCS5D02G537600	aspartokinase 1, chloroplastic-like	596	0	68.69	**8.62**	**4.45**	**9.11**	1.84	1.63E-37	2.03E-35	
TRAESCS1B02G138100	auxin-responsive protein IAA15	198	2E-143	81.71	**3.64**	1.88	**3.57**	**2.42**	1.56E-28	1.12E-26	
TRAESCS5A02G247200	glucose-6-phosphate isomerase 1, chloroplastic	614	0	93.86	**3.08**	1.57	**2.09**	-0.27	2.07E-28	2.68E-36	DEGs in red boxes of cluster 4 in Fig. 4I
TRAESCS4A02G002600	MADS-box transcription factor 47-like isoform X2	163	7E-116	92.93	**3.95**	0.66	**2.60**	**3.05**	0.000023	0.000247	
TRAESCS7D02G246600	probable histone H2A variant 3	139	3E-95	95.7	**2.08**	1.78	**3.65**	**2.75**	5.65E-47	1.47E-26	
TRAESCS6B02G466700	protein argonaute 1C-like isoform X2	1013	0	89.28	**5.24**	**2.58**	**4.52**	**5.89**	1.53E-64	8.82E-62	
TRAESCS6D02G293200	putative MADS-domain transcription factor	228	1E-167	96.69	**5.72**	**2.42**	**6.37**	**2.55**	1.46E-42	1.31E-43	
TRAESCS1B02G100800	RNA-binding protein 8A	209	9E-152	85.74	**4.77**	1.01	**4.64**	**2.08**	4.73E-34	2.42E-40	

TRAESCS1B02G105100	ribosome biogenesis protein NOP53	407	0	83.3	**4.30**	1.07	**6.42**	**2.08**	2.01E-38	4.76E-32
TRAESCS1B02G051600	uncharacterized protein LOC109787361	466	0	62.52	**6.65**	**9.45**	**5.94**	**3.47**	6.62E-46	1.2E-44

Bold numbers indicate more than two-fold changes in expression.

Table 2(on next page)

Table 2. List of diiferentially expressed protein kinase genes under salt stress condition

1 **Table 2:**

2 **List of differentially expressed protein kinase genes under salt stress condition.**

Gene ID	Description	Length	E-value	Similarity (%)	Log_2 fold change (PL6/PL1)				p-value	FDR
					0 h	3 h	12 h	24 h		
TraesCS1B02G098700	CBL-interacting protein kinase 17	466	0	89.58	**5.64**	1.70	**4.46**	1.42	3.76E-43	6.32E-41
TraesCS5B02G223900	CBL-interacting protein kinase 16	447	0	88.69	0.66	0.32	-0.20	−0.80	0.00187	0.011796
TraesCS4B02G319900	CBL-interacting protein kinase 9	443	0	94.32	1.37	0.71	0.36	0.35	4.87E-26	3.05E-24
TraesCS1B02G098600	CBL-interacting protein kinase 17	466	0	89.63	**5.45**	1.75	**6.91**	0.84	2.73E-25	1.65E-23
TraesCS5A02G492000	CBL-interacting protein kinase 9	446	0	94.25	0.72	0.47	0.04	0.28	8.66E-13	2.34E-11
TraesCS1D02G082500	CBL-interacting protein kinase 17	480	0	87.23	−0.21	0.29	−0.62	−0.89	3.29E-05	0.000341
TraesCS4D02G118500	CBL-interacting protein kinase 14	362	0	82.78	0.67	1.11	0.31	0.33	0.00488	0.026029
TraesCS1D02G082600	CBL-interacting protein kinase 17	448	0	86.72	0.36	0.01	−0.50	−0.37	6.13E-05	0.000598
TraesCS1A02G080600	CBL-interacting protein kinase 17	466	0	90.22	−0.39	−0.16	−0.76	−1.21	1.96E-07	0.000003
TraesCS1A02G080700	CBL-interacting protein kinase 17	471	0	89.6	−0.26	0.23	−0.86	−0.50	1.12E-10	2.52E-09
TraesCS4B02G120400	CBL-interacting protein kinase 14	444	0	92.95	−0.12	−0.80	0.86	0.38	0.000271	0.002245
TraesCS2D02G107100	CBL-interacting protein kinase 29	436	0	87.67	−0.24	−0.31	−0.51	0.08	0.005552	0.02886
TraesCS3B02G169300	CBL-interacting protein kinase 5	464	0	93.17	0.61	0.96	0.16	−0.54	4.65E-08	7.74E-07
TraesCS4D02G316500	CBL-interacting protein kinase 9	445	0	94.22	1.03	0.96	−0.10	0.27	3.23E-12	8.38E-11
TraesCS3D02G151500	CBL-interacting protein kinase 5	464	0	93.02	0.59	0.71	0.13	−0.26	2.39E-05	0.000254
TraesCS3A02G135500	CBL-interacting protein kinase 5	466	0	92.32	1.13	0.05	0.14	0.00	4.62E-06	5.69E-05
TraesCS1B02G104900	mitogen-activated protein kinase 14	549	0	92.96	**3.98**	1.64	**3.09**	1.98	6.05E-42	9.68E-40
TraesCS7A02G410700	mitogen-activated protein kinase 12	578	0	92.91	0.41	0.32	0.07	0.55	7.32E-06	8.69E-05

TraesCS5B02G075800	SNF1-type serine-threonine protein kinase	363	0	93.99	0.85	0.85	0.20	0.92	5.49E-05	0.000542
TraesCS5D02G081700	SNF1-type serine-threonine protein kinase	364	0	94.37	0.54	0.77	0.22	0.52	0.000294	0.002407
TraesCS1D02G308200	SNF1-related protein kinase regulatory subunit beta-1	280	0	82.88	−1.25	−0.65	0.17	0.67	7.37E-05	0.000706
TraesCS5A02G069500	SNF1-type serine-threonine protein kinase	360	0	95.18	−0.78	−0.29	−0.35	0.67	0.002772	0.01638

Bold numbers indicate more than two-fold changes in expression.

Table 3(on next page)

Table 3. List of differentially expressed salt stress responsive ggenes selected by MapMan program

Table 3:

List of differentially expressed salts stress responsive genes selected by MapMan program.

Gene ID	Description	Length	E-value	Similarity (%)	Log_2 fold change (PL6/PL1)				p-value	FDR	BinName from MapMan
					0 h	3 h	12 h	24 h			
TraesCSU02G196100	Pseudo-response regulator (PRR)	660	0	97.11	−0.67	−0.01	−0.99	**−4.44**	4.11E-07	5.98E-06	Circadian clock system
TraesCS5D02G078500	Kinesin-like protein KIN-12F isoform X2	3015	0	84.6	−0.73	−0.21	−0.05	**−2.42**	7.62E-15	2.4E-13	Cytoskeleton organization
TraesCS1B02G123200	Kinesin-like protein KIN-13A	519	0	92.31	**5.27**	2.00	**5.67**	**2.61**	1.73E-62	8.72E-60	Cytoskeleton organization
TraesCS1B02G024500	Actin-7	377	0	99.58	**4.70**	**4.81**	**5.63**	**2.86**	4.55E-63	2.37E-60	Cytoskeleton organization
TraesCS5B02G491800	Actin depolymerization factor-like protein	147	6.3E-104	88.78	0.86	−0.12	0.73	**−2.31**	1.92E-05	0.00021	Cytoskeleton organization
TraesCS5D02G492300	Actin depolymerization factor-like protein	147	6.3E-105	87.63	0.55	0.09	0.38	**−3.25**	2.08E-11	5.07E-10	Cytoskeleton organization
TraesCS1B02G069300	Protein unc-13 homolog	1107	0	93.26	**9.87**	**9.73**	**10.07**	1.73	1.97E-53	5.97E-51	Cell wall organization
TraesCS6D02G048900	Melibiase family protein	637	0	80.94	−2.04	**−3.80**	**−2.48**	−0.04	0.000177	0.001532	Cell wall organization
TraesCS1B02G084600	Hydroxyproline O-galactosyltransferase GALT3	591	0	83.91	**3.76**	**2.71**	**2.78**	0.79	5.51E-16	1.89E-14	Cell wall organization
TraesCS1D02G019000	Tricin synthase 1	248	1.8E-180	79.05	−1.48	0.37	**−2.29**	−0.17	6.39E-09	1.18E-07	Cell wall organization
TraesCS5D02G488900	Caffeic acid O-methyltransferase	353	0	86.01	−1.86	**−2.56**	**−4.53**	0.63	7.23E-20	3.17E-18	Cell wall organization

TraesCS1B02G098800	Acyl transferase 4	435	0	80.27	**8.49**	**2.00**	**8.69**	**2.57**	4.28E-31	3.63E-29	Cell wall organization
TraesCS3D02G116600	Alkane hydroxylase MAH1-like	517	0	88.56	0.02	0.08	**−2.60**	**−2.99**	0.001075	0.00741	Cell wall organization
TraesCS5D02G127300	Aldehyde dehydrogenase family 3 member H1-like	479	0	86.99	0.49	−0.29	**−2.17**	−1.78	2.63E-10	5.72E-09	Cell wall organization
TraesCS2A02G045800	GDSL esterase/lipase LTL1	369	0	90.05	**9.20**	1.62	**8.58**	**8.50**	3.69E-36	4.22E-34	Cell wall organization

Bold numbers indicate more than two-fold changes in expression.